

Cristian Marchioli 

Large-eddy simulation of turbulent dispersed flows: a review of modelling approaches

Received: 10 October 2016 / Revised: 23 December 2016
© Springer-Verlag Wien 2017

Abstract In large-eddy simulation (LES) of turbulent dispersed flows, modelling and numerical inaccuracies are incurred because LES provides only an approximation of the filtered velocity. Interpolation errors can also occur (on coarse-grained domains, for instance). These inaccuracies affect the estimation of the forces acting on particles, obtained when the filtered fluid velocity is supplied to the Lagrangian equation of particle motion, and accumulate in time. As a result, particle trajectories in LES fields progressively diverge from particle trajectories in DNS fields, which can be considered as the exact numerical reference: the flow fields seen by the particles become less and less correlated, and the forces acting on particles are evaluated at increasingly different locations. In this paper, we review models and strategies that have been proposed in the Eulerian–Lagrangian framework to correct the above-mentioned sources of inaccuracy on particle dynamics and to improve the prediction of particle dispersion in turbulent dispersed flows.

1 Introduction

Turbulent dispersed flows are multiphase flows in which a dispersed phase (particles, aerosols, droplets or bubbles) is transported and spatially distributed by a continuous fluid phase (gas or liquid). These flows are of paramount practical importance, as they are commonly encountered in a wide variety of environmental and industrial applications. Examples range from atmospheric pollutant dispersion and sediment transport in water bodies to dust/droplet separation, fibre suspensions, and spray combustion, to name a few. Turbulent dispersed flows are also very rich in physics, as they are characterized by a complex multi-scale interaction between the fluid turbulence and the particle distribution that still poses many challenging issues in terms of modelling, simulation, and experiments. A general overview of these issues is provided by a number of review papers [9, 49, 61, 144], to which the reader is referred for a comprehensive survey of the state of the art in the field.

Owing to the wide range of length- and timescales that characterize turbulent dispersed flows, several modelling approaches have been developed. Following the classification provided by Fox [35], the most detailed approach is based on direct numerical simulation of the microscopic governing equations (microscopic model, wherein both phases are fully resolved). This approach provides the information about the small-scale flow physics required to develop a continuum description of the flow based on suitable transport equations for low-order moments such as mass continuity and momentum conservation (macroscopic model). Macroscopic models can be developed using volume or ensemble averages of the microscopic governing equations (in this case, suitable closures for fluctuations are required). Alternatively, they can be developed by the formulation of an intermediate (mesoscopic) model that describes the mesoscale variables (e.g. velocity or volume) needed

C. Marchioli (✉)
Dipartimento Politecnico di Ingegneria e Architettura, Università di Udine, via delle scienze 206, 33100 Udine, Italy
E-mail: marchioli@uniud.it
Tel.: +39-0432-558006
Fax: +39-0432-558027

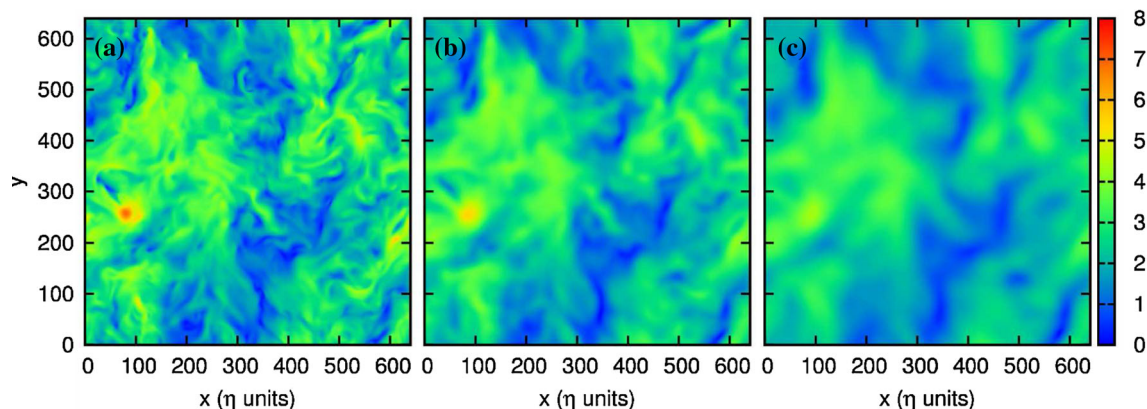


Fig. 1 Effect of filtering of the flow structures (identified by means of a 2D slice of the fluid vorticity) in HIT. **a** DNS, no filter applied, **b** LES with filter width $\Delta = 5\eta_K$, **c** LES with filter width $\Delta = 10\eta_K$, where η_K is the Kolmogorov length scale. The progressive loss of small-scale details of the flow, which are not felt by the Lagrangian particles as they evolve within the fluid domain, is apparent. Reprinted from [18]

to describe the physics of the dispersed phase in terms of kinetic equations. The macroscopic model is then obtained from the mesoscopic model using an averaging procedure to obtain the moments of the density function appearing in the kinetic equations (for instance, the zero-order moment of the density function is related to concentration, the first-order moment to the mean momentum) [35]. Recent work [82,83] has shown that particle kinetic variables alone are not sufficient to ensure well-posedness of the model: Rather, extended formulations, in which additional variables related to the underlying turbulent flow (like the fluid velocity seen by a particle along its trajectory) appear in the particle state vector, should be adopted in line with what is currently done in Lagrangian formulations [82,83,86]. Such hierarchical structure is the starting point for several simulation techniques, which are discussed at length in [35]. Here, we are interested in Euler–Lagrange (EL) simulations based on large-eddy simulation (LES) of turbulence. The reader is referred to [124] for a comprehensive account of the theoretical foundation, modelling issues, and numerical implementation of the Eulerian–Lagrangian approach for multiphase flows in this context. LES has emerged as a powerful simulation technique that allows lower computational cost compared with microscopic models based on direct numerical simulation (DNS) while retaining good statistical accuracy. This is because LES is based on the concept of spatial filtering, by which a low-pass filter is applied to separate the flow into large-scale motions that are directly computed (resolved on the computational grid using filtered flow equations) from small subgrid scale (SGS) motions whose effects are modelled [97]. A visualization of LES spatial filtering effects is provided in Fig. 1, which shows the impact on the flow structures in homogeneous isotropic turbulence (referred to as HIT hereinafter) for different filter widths [18].

The use of LES is particularly justified in practical applications dealing with turbulent flows (shear-dominated flows [94] or reacting flows controlled by large-scale mixing [95], in particular), where the statistical properties of the larger and most energetic scales are of interest. In order to accurately describe the large scales, one must model the small scales in a faithful way. Due to the complex statistical properties of turbulence, many models and methodologies have been proposed in the past (see [35,68,78,80,94–96] for a comprehensive review). While none of the models is proposed can be considered as a substitute for DNS, still the performance of some models can be considered fairly accurate: For instance, as far as the most common Eulerian turbulence statistics in flows where the rate-controlling processes occur in the resolved large scales are concerned [47,96]. Modelling capabilities are much less established in flows where these processes occur at the smallest scales (e.g. molecular mixing and chemical reactions in turbulent combustion at high Reynolds and Damkohler numbers [67,88,95,96,103,104], droplet break-up in liquid spray atomization at high Weber number [7,15] or momentum transfer in near-wall flows at high Reynolds number [58,96]).

In this review, we focus on LES modelling for two-phase dispersed flows, where the dynamics of the dispersed phase is intricately linked to the interplay that occurs between particles and turbulence at the particle scale [20,48,74,120]. Modelling issues arise when spatial filtering affects such interplay, preventing particles from interacting with the unresolved SGS structures. As a result, particle trajectories in LES fields progressively diverge from those that would have been obtained in a laboratory experiment or in DNS (regarded as exact numerical experiment [76]). In the EL framework, trajectory divergence is mainly due to inaccurate estimation

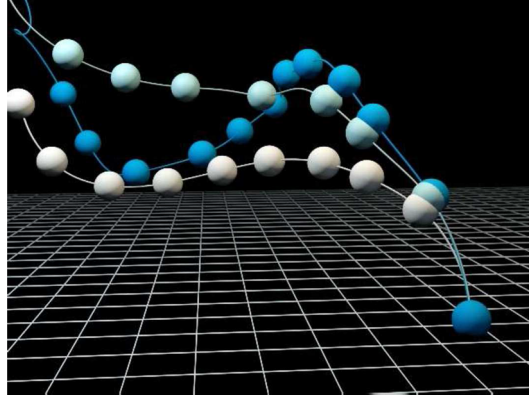


Fig. 2 Deviation of particle trajectory in coarse-grained HIT flow fields. *Blue* particle trajectory in DNS. *Cyan* particle trajectory in LES with filter width $\Delta = 5\eta_K$, corresponding to a grid coarsening factor $CF = 2$ with respect to DNS. *White* particle trajectory in LES with filter width $\Delta = 10\eta_K$ ($CF = 4$) (colour figure online)

of the forces acting on the particles and leads to a progressive loss of correlation between the flow field that particles see in LES and the flow field they would see in DNS. This is nicely exemplified in Fig. 2, which shows the diverging trajectories of one sample particle in the same fine- and coarse-grained flow fields of Fig. 1. Modelling issues become particularly challenging in the case of particle-laden wall-bounded flows, where closure problems arise in viscosity-dominated regions with strong turbulence inhomogeneity and anisotropy. In such regions, the complex phenomenology of the flow prevents the use of simple SGS models to predict the effect of the unresolved flow scales on crucial phenomena such as dispersion, deposition and resuspension [98]. A common approach, valid also for RANS [30,83], has been to extend models developed for simpler, free-shear flows by incorporating the effect of near-wall gradients of turbulence intensity [81]. As we will try to highlight in the following, however, direct extensions not grounded on well-established first principles may easily produce poor results.

1.1 Governing equations and relevant modelling parameters

In the simplest situation, particles are treated as material points with density much higher than that of the fluid (mimicking gas–solid or gas–liquid flows) and size much smaller than the smallest resolved length scale of the flow (particles can thus be bigger than the Kolmogorov scale: This makes point-particle LES very attractive for the investigation of high Reynolds number turbulence [10]). The corresponding equations of particle motion are [38,79]:

$$\ddot{\mathbf{x}}_p = \dot{\mathbf{v}}_p = f_D(\mathbf{u}_s - \mathbf{v}_p)/\tau_p \quad (1)$$

where $\mathbf{x}_p = \mathbf{x}_p(t)$ is the instantaneous particle position, $\mathbf{v}_p = \mathbf{v}_p(\mathbf{x}_p, t)$ is the instantaneous particle velocity, f_D is a drag correction factor that depends on particle inertia, $\mathbf{u}_s = \mathbf{u}_f(\mathbf{x}_p, t)$ is the instantaneous fluid velocity \mathbf{u}_f evaluated at the particle position (referred to as *velocity seen* hereinafter), and

$$\tau_p = \frac{\rho_p d_p^2}{18\mu} \quad (2)$$

is the particle relaxation time (a measure of the timescale of momentum transfer between the particle and the surrounding fluid). The fluid velocity seen can be decomposed as $\mathbf{u}_s = \bar{\mathbf{u}}_s + \mathbf{u}'_s$, where $\bar{(\cdot)}$ represents a spatially smoothed value in LES (or an averaged value in RANS or PDF statistical closures) and \mathbf{u}'_s is the subgrid (or fluctuating) part of \mathbf{u}_s . With reference to Eq. (1), all modelling issues in the EL framework are related to the estimation of \mathbf{u}_s (or, as discussed in Sect. 3, \mathbf{u}'_s according to the specific model formulation adopted), which is fully available only in DNS. Yeh and Lei [138,139] were the first to investigate particle dispersion in turbulent flow using LES. These authors assumed the effect of subgrid fluid turbulence on particle dynamics to be negligible and solved for Eq. (1) using the filtered fluid velocity provided by LES. Other works followed (see [6,7,26,27,66,69,70,131,132] among others), which were based on the same assumption. As discussed in Sect. 2, however, the influence of the unresolved scales cannot be neglected unless the fraction of energy

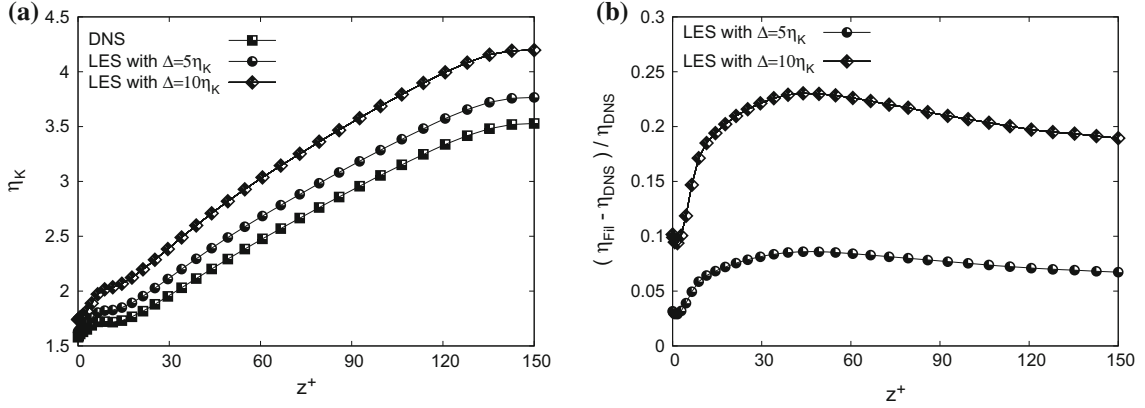


Fig. 3 Effect of filtering on the smallest resolved length scale η in turbulent channel flow (shown as a function of the wall-normal coordinate, z). **a** Effect of filter width (*square* DNS, *circle* LES with filter width $\Delta = 5\eta_K$, *downtriangle* LES with filter width $\Delta = 10\eta_K$), **b** nondimensional filtered-to-unfiltered scale ratio, $(\eta_{\text{fil}} - \eta_{\text{DNS}}) / \eta_{\text{DNS}}$. Reprinted from [18]

removed from the fluid velocity field is small (namely, the LES is well-resolved [8]). In fact, several studies have shown that subgrid fluid velocities must be taken into account to provide reliable calculations of particle kinetic properties and/or preferential concentration phenomena [61, 83]. The first formulation of particle SGS model accounting explicitly for \mathbf{u}'_s in Eq. (1) was proposed by Wang and Squires [131] (see Sect. 3 for details). Since this early and simple closure, which proved to have minimal influence on particle statistics when applied in turbulent channel flow, many other proposals have been made [83]. These will be recalled in Sect. 3, while their application to particle-laden flow is thoroughly discussed in Sect. 4.

To understand the conceptual difficulties associated with the development of SGS closures for the Lagrangian equation of particle motion, we remark here that, while in DNS the only length scales that characterize particle dispersion in turbulent flows are the particle diameter d_p , the size l of the large-scale eddies, and the Kolmogorov length η_K , in LES an additional scale must be considered: the filter width Δ , which determines the smallest characteristic length of the resolved turbulence structures. Figure 3 shows the wall-normal behaviour of η_K , in turbulent channel flow (data are taken from the same database described in [18], with filter widths $\Delta = 5\eta_K$ and $\Delta = 10\eta_K$). In this case, filters of increasing width are applied to DNS fields in a priori tests. The length scale increases with Δ , and the increase is higher in the centre of the channel than near the walls, in both absolute (Fig. 3a) and relative (Fig. 3b) terms. This means that filtering removes more “information” in the centre of the channel, where particles become exposed to a narrower range of flow scales (read structures), thus leading to under-prediction of pair separation over short times, as demonstrated in [18]. Timescales are also crucial: These are the particle relaxation time and the characteristic flow timescale (for instance the eddy turnover time). Their ratio defines the scale-dependent Stokes number $St = \tau_p / \tau_f$ and determines the range of eddies for which the particles behave as tracers (this happens when $St \ll 1$).

Following [10, 125], two types of SGS effects can be observed in LES of turbulent dispersed flows: the effect of the subgrid turbulence on particle dynamics, which occurs in one-way coupling regimes, and the effect of the energy transferred from the particles to the fluid, which may cause significant variations of SGS momentum (and therefore turbulence modulation) under sufficiently large mass loading (two-way coupling regime). To characterize these effects in the one-way coupling regime, a subgrid Stokes number can be conveniently defined as [10, 125]:

$$St_{SGS} = \tau_p / \tau_\Delta \quad (3)$$

where $\tau_\Delta \sim (\Delta^2 / \epsilon)^{1/3}$ is the cut-off timescale and ϵ is energy dissipation. The value of St_{SGS} is intermediate between $St_l = \tau_p / \tau_l$, which is the minimum value of St based on the turnover dynamics of the large eddies ($\tau_l = l / u_l$ with u_l the turnover velocity of the large eddies), and $St_K = \tau_p / \tau_K \gg St_l$, which is the maximum value of St based on the Kolmogorov timescale τ_K . Note that $St_K / St_l \sim Re_l^{1/2}$, where $Re_l = u_l l / \nu$ with ν the fluid kinematic viscosity.

When $St_{SGS} \ll 1$, particles are SGS-non-inertial with respect to subgrid eddies (here we adopt the terminology of [125]): They are sensitive to the high-frequency fluctuations of subgrid turbulence (which are filtered) while behaving as tracers with respect to the large eddies. In this limit, which is encountered, for instance, in solar-power receivers (where $St_K \sim \mathcal{O}(1)$ and $St_l \ll 1$), a particle SGS model is required to

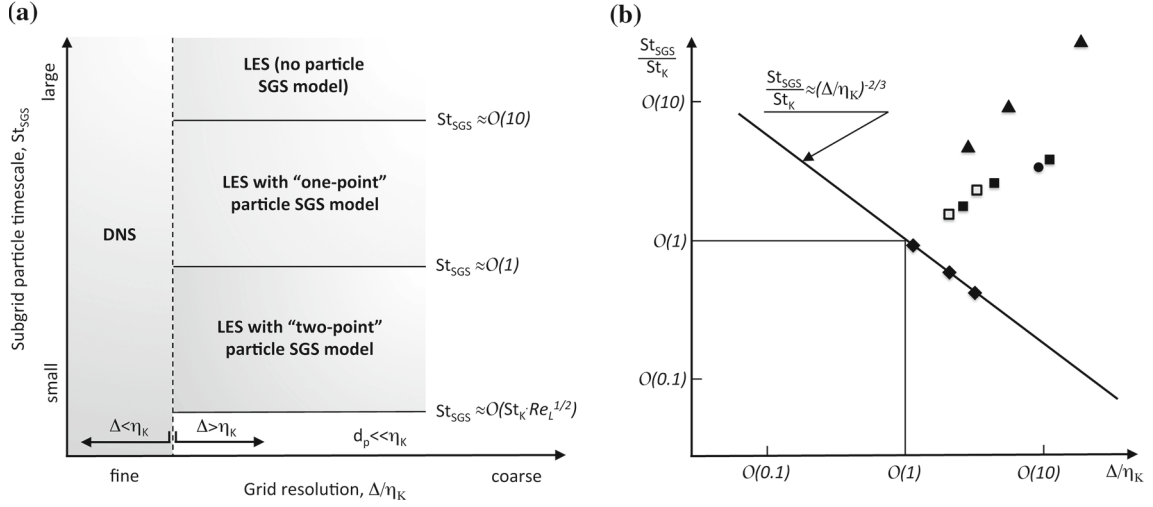


Fig. 4 a Conceptual classification of Eulerian–Lagrangian modelling approaches to the simulation of particle-laden flows as a function of two parameters: The subgrid particle timescale, St_{SGS} , and the ratio between the grid resolution and the Kolmogorov length scale, Δ/η_K . Solid and dashed lines in this panel are simply conceptual dividers. **b** Sample database of simulation results from archival literature. Symbols refer to different studies and different flow configurations: Marchioli et al. [72, 73] (*filled squares*) channel flow at shear Reynolds number $Re_\tau = 150$ based on the half channel height); Innocenti et al. [51] (*open squares*, channel flow at $Re_\tau = 300$); Fede and Simonin [31] (*diamonds*) HIT at Taylor-microscale Reynolds number $Re_\lambda = 34.1$); Gobert and Manhart [44] (*circles*) HIT at $Re_\lambda = 52$); Cernik et al. [21] (*triangles*) decaying HIT with initial $Re_\lambda = 74$). The thick solid line in panel (b) represents the dependence of the parameter St_{SGS}/St_K on Δ/η_K that can be derived in HIT

solve Eq. (1). Particles follow the motion of the large eddies but slip predominantly on the small ones: This dynamics is characterized by particle-to-fluid relative velocities much smaller than u_l and hence by small particle Reynolds numbers. In the following, we will focus on the models that have been developed in this regime (see [31, 55, 62, 117] among others). In the opposite limit ($St_{SGS} \gg 1$), particles become SGS-inertial with respect to subgrid eddies [125], and (in principle) no particle SGS model is necessary: The dominant eddies controlling the relative velocity are resolved in LES, and the corresponding velocity \bar{u} is enough to solve Eq. (1) [10]. This limit is typical of droplet dispersion in most spray-combustion applications: Droplets are characterized by $St_l \sim \mathcal{O}(1)$, particle-to-fluid relative velocities comparable to u_l and particle Reynolds numbers determined by the integral scales of the turbulent flow [125].

These considerations apply to sub-Kolmogorov particles ($d_p \ll \eta_K$) that are characterized by a density much higher than that of the fluid. In this limit, a conceptual classification of the different modelling approaches to the numerical simulation of particle-laden flows is proposed in Fig. 4a, together with a collection of sample results available in archival literature, displayed in Fig. 4b. The subgrid particle timescale, as defined in Eq. (3), and the grid resolution (which can be assumed equal to the filter width in the case of LES) normalized by the Kolmogorov length scale, Δ/η_K , are the parameters taken into account. It can be easily demonstrated that, in homogeneous isotropic turbulence, these quantities obey the following scaling law: $St_{SGS}/St_K = \tau_K/\tau_\Delta \simeq (\Delta/\eta_K)^{-2/3}$, which can be used to estimate St_{SGS} based on the filter width used in LES. When $\Delta > \eta_K$ and St_{SGS} is large (order 10 or higher in the figure), particles are SGS-inertial, and no SGS model is required to track their trajectory in LES fields. For smaller values, particles are SGS-non-inertial, and a particle SGS model becomes necessary: A “one-point” model (capable of reproducing one-point particle statistics) is sufficient when the order of magnitude of St_{SGS} is between 1 and 10, whereas a “two-point” model (capable of reproducing two-point particle statistics and correlation timescales) is deemed necessary. Clearly, the quantitative determination of the threshold values at which specific models should be used depends on the observables of interest and the degree of accuracy required, so Fig. 4a is intended for conceptual use only. Figure 4b serves the purpose of visualizing how previous studies fill the $(St_{SGS}/St_K; \Delta/\eta_K)$ parameter space for both HIT and channel flows.

Size effects on heavy particles become important only for extremely high values of the Kolmogorov-based Stokes number St_K . However, this is a situation of limited interest for turbulent dispersed flows since particle dispersion would be conditioned almost entirely by the initial velocity of the particles [125]. As far as finite-size effects ($d_p \sim \eta_K$) in the one-way coupling regime are concerned, situations of practical interest are those characterized by $St_l \sim \mathcal{O}(1)$ (or smaller) when the Reynolds number is of order $Re_l \sim (l/\Delta)^{4/3}(\rho_p/\rho)^2$

or higher. In this case, the subgrid Stokes number is small ($St_{SGS} \leq 1$), and small are the particles with respect to the filter width, due to the large-scale separation of the flow [125]. In such St_{SGS} range, particles are SGS-non-inertial, and modelling of subgrid fluid velocity fluctuations is necessary. In addition, wake dynamics becomes more chaotic, and the particle Reynolds number increases: Fluid inertia becomes important, possibly in combination with additional effects due to significant velocity gradients at the particle level. Corrections to the expression of the drag acting on the particles are therefore needed [125].

In the two-way coupling regime, the importance of SGS effects can be estimated considering an alternative expression of the subgrid Stokes number defined in Eq. (3) [10, 125]:

$$St_{SGS} = (l_*/\Delta)^{2/3} \quad (4)$$

where $l_* \sim (\tau_p^3 \epsilon)^{1/2}$ yields an estimate of the size of the eddies for which the particle-to-fluid relative velocity is maximum. Equation (4) provides a direct indication of whether the characteristic flow scale at which the two-way coupling takes place is resolved or, rather, falls in the subgrid range. In particular, particles are SGS-inertial with respect to the subgrid eddies when $St_{SGS} \gg 1$ and the mass loading ratio (defined here as the total mass of the particles divided by their total mass of the fluid) is $\alpha \sim \mathcal{O}(1)$: In this case, subgrid modelling is not required since inter-phase coupling is stronger with respect to the resolved eddies. At the other extreme, namely $St_{SGS} \ll 1$ and $\alpha \sim \mathcal{O}(1)$, particles are SGS-non-inertial with respect to the subgrid eddies (while behaving as tracers with respect to the resolved scales), and inter-phase coupling takes place preferentially in the subgrid range. Additional modelling of the subgrid fluid velocity fluctuations is thus required to compute the transfer of momentum (and energy) from the particles to the fluid [125]. In the following, we will focus our review on the one-way coupling regime since this is the regime considered in the vast majority of archival literature.

1.2 A visual description of modelling issues in LES with particles

To understand the modelling challenges posed by the LES framework in the one-way coupling regime, we can refer to Fig. 5: This figure compares the time-averaged one-dimensional wavelength (Fig. 5a) and wavenumber (Fig. 5b) spectra of the fluid kinetic energy obtained from DNS and LES of the same flow field (turbulent channel flow). In particular, spectra are taken at a distance of 5 viscous units from the wall at $Re_\tau = 150$ and are shown here in a log-log plot. As is well known, LES produces a deficit in the energy spectra, which is the signature of missing scales (structures) in the flow field and can be decomposed into two contributions. One is clearly the energy associated with the unresolved (subgrid) scales removed by cut-off. The other, with the obvious exception of the cut-off filter, is the energy that filtering may subtract from the resolved scales, corresponding to the gap between the LES spectrum and the DNS spectrum above the cut-off, where wavelengths are smaller than $k_c \propto 1/\Delta$ in Fig. 5a, and frequencies are smaller than $\omega_c \propto 1/\tau_\Delta$ in Fig. 5b. A first issue at stake is that recovering the energy deficit to match the level of fluid and particle velocity fluctuations in DNS does

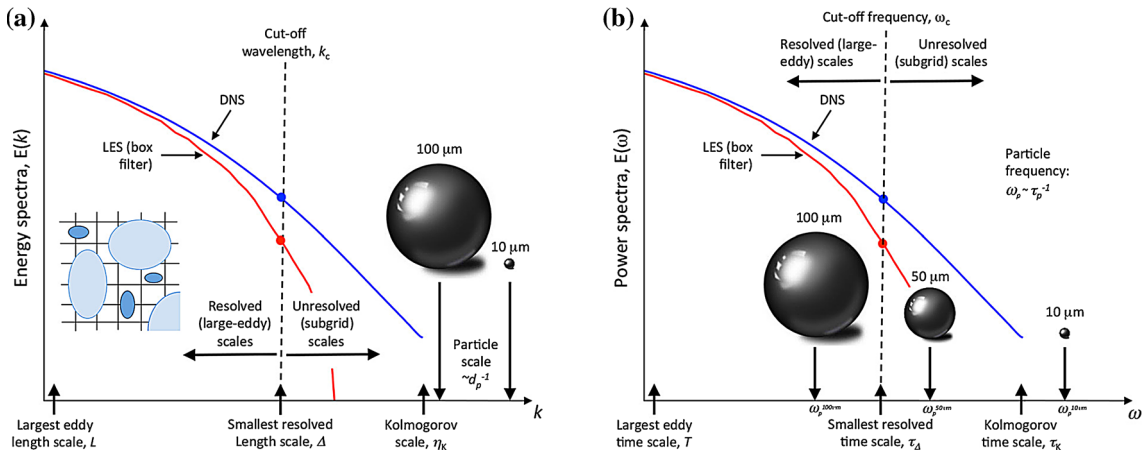


Fig. 5 Comparison between DNS and LES one-dimensional streamwise energy spectra: **a** wavelength spectra, **b** wavenumber (frequency) spectra

not ensure a quantitative replica of the SGS turbulence effects on near-wall accumulation and local particle segregation [72,73]. A second modelling issue is that, even if there is separation of length scales between particles and fluid, filtering may remove precisely the structures with characteristic timescale comparable to the particle timescale: These structures are of particular importance because of their predominant role in determining preferential concentration [9,33,71,93,112]. As shown in Fig. 5a for channel flow, the particle length scale is well separated from the smallest flow length scale (namely d_p smaller than the Kolmogorov length η_K) in the point-particle limit. For instance, 100 μm particles can be safely considered microscale being smaller than η_K , but also significantly smaller than Δ . However, there is no separation of timescales between particles and fluid (meaning that $\tau_p > \tau_K$) unless particles are really small, e.g. the 10 μm particles in Fig. 5b. In this figure, the estimated particle response frequencies are proportional to $1/\tau_p$, and the particle-to-fluid density ratio is fixed (the typical reference case being gas–solid flow, where $\rho_p/\rho \gg 1$). The 10 μm particles can still be considered microscale and SGS-non-inertial with respect to subgrid eddies. However, they do not exhibit strong preferential concentration because of their weak inertia and are not much influenced by SGS effects. On the other hand, the 100 μm particles preferentially interact with eddies in the resolved range, but their subgrid Stokes number is $St_{SGS} \sim \mathcal{O}(1)$, indicating possible influence also from the unresolved scales. An interesting situation is observed for particles with an intermediate size (50 μm in diameter): These particles interact preferentially with eddies in the subgrid range, and a strong effect of filtering on their tendency to cluster within the flow should be expected. This observation is in qualitative agreement with the results of Fede and Simonin [31] and Ray and Collins [107], who showed that filtering reduces clustering for particles with small inertia (small Stokes number) but increases clustering for particles with high inertia (high Stokes number). This finding is explained considering that, for fixed density ratio, particle inertia depends directly on particle size, and filtering removes primarily the eddies with which small particles tend to interact. This has a direct effect on preferential concentration of such particles. On the other hand, subgrid eddies have a randomizing (mixing) effect of the spatial distribution of large particles: When these eddies are removed by filtering, mixing is partially prevented, and clustering is favoured.

1.3 Criteria for assessment of modelling approaches

One important aspect in the formulation of modelling approaches to LES of turbulent dispersed flows is the choice of the criterion used to judge the quality of the model and to appraise its merits relative to other models. Currently, there are two different types of criteria. One is aimed at assessing the capability of the model to reproduce with accuracy one-point statistical moments (such as dispersion coefficients and particle kinetic energy), which is what one typically requires from Langevin-type models. The other is aimed at assessing the capability of the model to reproduce instantaneous spatial distributions and geometrical features of particle dispersion (such as those related to the preferential concentration phenomena described in Sect. 2). This type of information is what one would typically require from structural models, described in Sect. 3. An ideal model (not yet available on the market, unfortunately) should be able to satisfy both criteria, but in most situations models are assessed only with respect to one of them. Therefore, the choice of the model depends on the specific quantities that must be predicted and/or reconstructed.

2 Particle transport mechanisms in turbulent dispersed flows and impact of LES filtering

In this section, we provide a brief overview of the transport mechanisms that govern turbulent particle dispersion and lead to preferential concentration of inertial particles. The reader is referred to [120,122] for a more detailed presentation of these mechanisms. We focus on wall-bounded flows, where preferential concentration leads to well-known particle deposition, accumulation and clustering phenomena. We also discuss the effect that spatial filtering has on the capability of LES to reproduce quantitatively transport phenomena. Understanding the impact of filtering is crucial to devise efficient SGS models for Lagrangian particle tracking (LPT), but also very important for improving successive model parameterization in terms of characteristic timescale, Stokes number, and Reynolds number dependence, etc. This explains the great deal of effort devoted to quantification and analysis of the errors introduced by the lack of SGS scales on particle dynamics in recent years (see [8,13,16,18,31,39,44,56,72,73,100,101,107,110,113] among others). Even in the ideal case in which LES of the fluid phase could provide the exact dynamics of the resolved scales, two sources of errors would still persist. One is the *pure filtering error*, associated with the use of the filtered fluid velocity in Eq. (1): This error has been shown to provide inaccurate estimation of the forces acting on particles [13,39]. The second

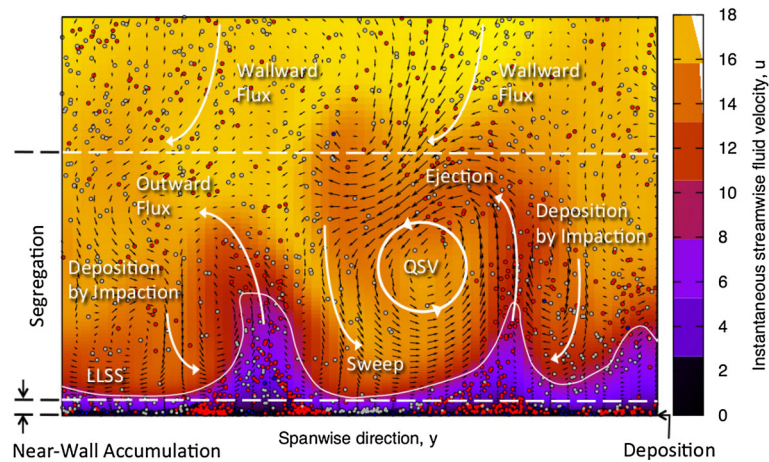


Fig. 6 Illustration of transport mechanisms driving concentration build-up in the near-wall region of turbulent bounded flow. Reprinted from [121]

source of error is associated with the time accumulation of the pure filtering error and leads to the divergence of trajectories shown in Fig. 2: In LES, therefore, the forces considered in Eq. (1) are evaluated at locations that are increasingly far from those that would be occupied at the same time step (and starting from the same initial position) in a companion DNS. We remark here that the effects of these two errors on particle concentration and velocity statistics cannot be singled out easily. Attempts have been made only for somehow idealized situations, e.g. pair separation of tracer particles in a priori LES of HIT [18].

Turbulent transport mechanisms are crucial to many industrial and environmental applications, involving, for instance, mixing, combustion, depulveration, spray dynamics, pollutant dispersion and cloud dynamics [120]. This is because they dictate the space distribution attained by the particles, which is the key information sought in most of the processes. In turbulent dispersed flows, however, particle distribution becomes strongly non-homogeneous as soon as particle inertia becomes significant. Particles sample preferentially the periphery of strong vortical regions and segregate into straining regions as a result of their interaction with the vortical coherent structures that control all transfer processes (for both the carrier phase and the dispersed phase) [9,20,48,71,74,120,122,128]. A snapshot of such interaction is provided in Fig. 6 (adapted from [120]), obtained from a DNS of particle-laden turbulent channel flow. Figure 6 shows a cross-flow view of particles (drawn as circles) and coherent flow structures. To highlight the correlation between particles and structures, we discriminate between particles moving away from the wall in the wall-normal direction (in red), particles moving towards the wall (in grey) and particles with nearly zero wall-normal velocity (in blue). Ejections of low-momentum fluid and wall-ward sweeps of high-momentum fluid can be observed at the sides of a quasi-streamwise vortex (QSV), flanked by lifted low-speed streaks (LLSS) of fluid. In the same figure, we illustrate the underlying transport mechanisms. To reach the accumulation and deposition regions, particles must first form coherent clusters in regions of the buffer layer where sweeps can entrain them. Particles entrained in a sweep are brought to the near-wall accumulation region, where particle concentration typically reaches its maximum. In the case of inertial particles evolving in non-homogeneous turbulent flow, such drift is driven by turbophoresis (a mechanism first identified by [19,108] and later investigated in many experimental and numerical studies: see [120] for a review). Once in the accumulation region, embedded well into the viscous layer, particles may either deposit at the wall or be re-entrained into the outer flow by ejections [128]. Deposition may occur by impaction when particles acquire enough momentum to coast through the accumulation region and deposit directly, or by diffusion-like mechanisms when deposition is driven by the residual near-wall turbulent fluctuations that, due to flow non-homogeneity, are always stronger in transporting particles to the wall. Re-entrainment may occur when particles are resuspended by the same vortex that brought them to the wall; otherwise, particles remain trapped for long times inside the viscous layer [93,121]: Eventually, the higher intensity of particle transfer fluxes to the wall leads to the well-known concentration build-up in bounded flows.

Based on current understanding of particle transport in turbulent flows, it appears clear that reliable predictive models for engineering and/or physical applications should be able to reproduce turbophoresis [62,63,73,77,83,131]. This implies accurate characterization of the flow field (which the coarse-grained filter-

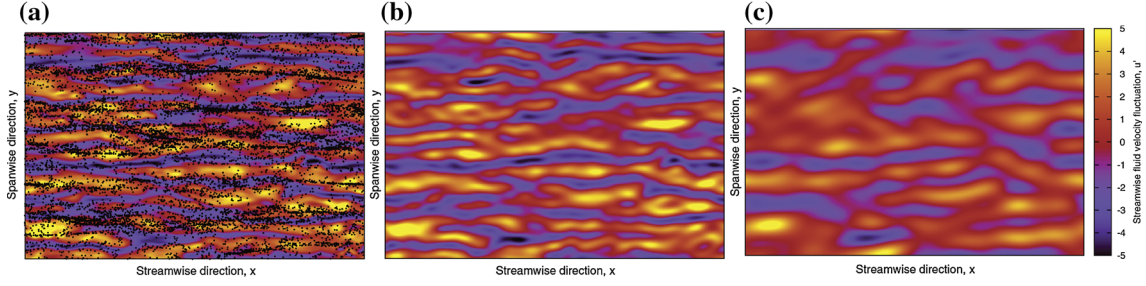


Fig. 7 Effect of filtering on near-wall low-speed streaks in turbulent channel flow. Particle segregation into low-speed streaks as obtained from DNS is shown in **a**. Rendering of the streaky structure deteriorates when spatial filtering is applied and the flow field becomes coarse-grained, as shown in **b**, **c** for grid coarsening factor $CF = 4$ and 8 , respectively. Reprinted from [13] with the permission of AIP Publishing

ing of the smallest flow scales by LES does not always grant) and of the particle–turbulence interaction at the particle scale. This is particularly important in the near-wall region where the physical mechanisms depicted in Fig. 6 give rise to complex segregation dynamics that collect particles in the low-speed regions of the viscous layer. Visual evidence of this process is given in Fig. 7a. As shown in Fig. 7b, c, however, filtering acts to smooth streaks out, thus attenuating the fluid velocity fluctuations and increasing the streamwise fluid velocity seen. This combines with a decrease in wall-normal velocity seen near the wall, leading to reduced turbophoretic drift [13] and to coarsened patterns in preferential concentration [98]. An additional complicative aspect is that the selectivity of particle–turbulence interaction, and hence, the relative importance of segregation, deposition and re-entrainment mechanisms depend on particle inertia [48, 74].

Among the many other investigations on the influence of subgrid fluid turbulence, there is general agreement about the lack of significant effects on one-point particle statistics (e.g. particle dispersion, particle Lagrangian timescale, particle velocity fluctuations). In addition, Fede and Simonin [31] have shown that, in homogenous isotropic turbulence (at $Re_\lambda \simeq 34$), the inclusion of subgrid effects on particle dispersion changes the dispersion coefficient by less than 2% if $\kappa_c L_f > 10$, where κ_c is the cut-off wavenumber and L_f is the integral length scale of the fluid. A similar conclusion was drawn by [8] for channel flow. However, important phenomena such as particle preferential concentration, particle wall accumulation, and inter-particle collisions turn out to be much more sensitive to filtering. Figure 8 shows the effect of subgrid turbulence on particle segregation resulting from preferential concentration in HIT (panel a) and on collision timescale (panel b) at varying particle inertia.

In Fig. 8a, segregation is quantified by the deviation from randomness, a box-counting parameter defined as:

$$\Sigma_p = \frac{\sigma - \sigma_{Poisson}}{\lambda} \quad (5)$$

where σ is the standard deviation of the probability density function of particle spatial distribution within the flow, $\sigma_{Poisson}$ is the standard deviation of the Poisson distribution (corresponding to a random spatial distribution of particles), and λ is the mean number of particles per cell. The larger Σ_p , the larger the deviation of the actual particle distribution from a random one. In Fig. 8a, the ratio $\Sigma_{p, filt} / \Sigma_p$ between the deviation from randomness in filtered LES fields, $\Sigma_{p, filt}$, and the deviation from randomness in DNS fields, Σ_p , is considered. Clearly, $\Sigma_{p, filt} / \Sigma_p < 1$ (resp. > 1) means that particle segregation in filtered fields is lower (resp. higher) than in unfiltered fields. The effect of filtering on segregation is examined at varying particle inertia, quantified by Fede and Simonin [31] using a subgrid Stokes number based on the Lagrangian integral timescale of the subgrid fluid velocity seen by an inertial particle along its trajectory, $T_{L,SGS}^{@p}$ ¹ rather than on τ_Δ as done in Eq. (3): Hence, $St_{SGS}^* = \tau_p / T_{L,SGS}^{@p}$. Figure 8a shows that:

- for subgrid Stokes number $St_{SGS}^* > 5$ segregation is unaffected by subgrid turbulence (this is because particle inertia is high enough to have segregation controlled by the large energy-containing eddies in the flow, which are only slightly affected by filtering);

¹ The Lagrangian integral timescale of the subgrid fluid velocity seen by an inertial particle along its trajectory is defined as follows: $T_{L,SGS}^{@p} = \int_0^\infty R_{L,SGS}^{@p}(\tau) d\tau$, where $R_{L,SGS}^{@p}(\tau) = \frac{\langle u'_{s,i}(t_0)u'_{s,i}(t_0+\tau) \rangle}{\langle u'_{s,i}(t_0)u'_{s,i}(t_0) \rangle}$ is the subgrid fluid velocity correlation seen by an inertial particle.

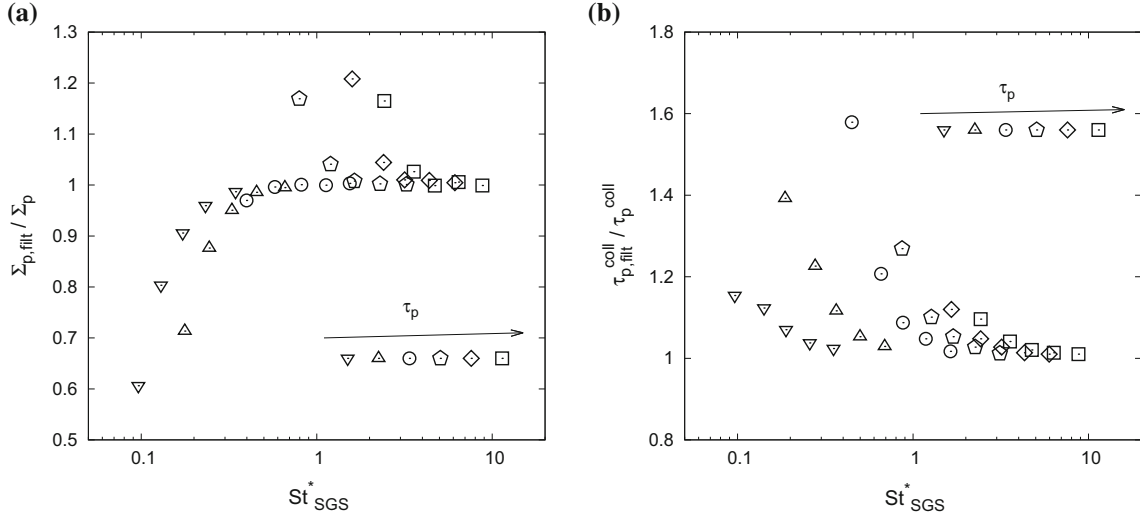


Fig. 8 Effect of filtering on particle segregation (a) and on inter-particle collision timescale (b) in homogeneous isotropic turbulence, as a function of the subgrid Stokes number, $St_{SGS}^* = \tau_p / T_{L,SGS}^{@p}$. Symbols represent increasing values of the particle relaxation time, namely of particle inertia. Plots redrawn from [31] with the permission of AIP Publishing

- for $0.5 < St_{SGS}^* < 5$ subgrid turbulence has a non-negligible effect on segregation that results in a randomization of particle distribution given by particle interaction with the energy-dissipating eddies;
- for $St_{SGS}^* < 0.5$ segregation is dominated by the unresolved flow scales, and one-point Lagrangian stochastic models are deemed inadequate to properly account for the influence of subgrid turbulence on particle motion.

A very useful *rule of thumb* proposed by [31], which agrees in spirit with the classification provided in Fig. 4a, is that no particle SGS model is needed in the particle motion equations when both conditions $\kappa_c L_f > 10$ and $St_{SGS}^* > 5$ are met. We remark here that the same trend shown in Fig. 8a has been observed in particle-laden turbulent channel flow (see e.g. [73]), where filtering decreases the fluid velocity fluctuations and, in turn, the particle velocity fluctuations, leading to a significant underestimation (resp. overestimation) of the segregation parameter below (resp. above) a certain threshold value of the particle Stokes number. Surprisingly, inaccuracies were observed also for small amounts of the filtered fluid velocity fluctuations, namely in well-resolved LES [73].

In Fig. 8b, inter-particle collisions are parameterized by the collision timescale, a measure of the collision rate:

$$\tau_p^{col} = \left[\frac{1}{2} \frac{N_p}{V_f} d_p^2 g_0 \langle |w_r| \rangle \right]^{-1} \quad (6)$$

where N_p is the total number of particles in the domain, V_f is the volume of the domain, g_0 is the radial distribution function, and $\langle |w_r| \rangle$ is the mean relative radial velocity. Figure 8b shows that the subgrid collision timescale $\tau_{p, \text{filt}}^{col}$ increases with respect to the *unfiltered* timescale τ_p^{col} for $St_{SGS}^* < 0.5$: Collisions become more rare as a result of a decrease in particle segregation combined with a reduction in mean radial relative velocity measured in filtered flow fields. For intermediate subgrid Stokes numbers, the collision timescale also increases, indicating that the decrease in $\langle |w_r| \rangle$ observed in the range $0.5 < St_{SGS}^* < 5$ prevails on the increase in segregation already discussed in Fig. 8a. Similar results were obtained by Jin et al. [53], who indicate a threshold value of $St_{SGS}^* \simeq 3$ below which the effects of the SGS motions on the turbulent collision of heavy particles must be included in the particle SGS model. Above this value, the overall collision rate was found to be reasonably predicted in both filtered DNS and LES [53].

In a series of recent works [13, 23, 39], these effects on particle dynamics have been revisited for the case of bounded flows in terms of the pure filtering error incurred when LPT is performed in LES fields. In [13, 23], this error has been computed as $\delta \mathbf{u} = \mathbf{u}_s - \bar{\mathbf{u}}_s$, assuming that all other sources of error affecting particle tracking in LES (modelling and numerical errors) can be neglected, including time accumulation of $\delta \mathbf{u}$: This is obtained by forcing particles to evolve in filtered DNS fields along the same trajectory that they would have followed if tracked in DNS fields [13]. As a result, $\delta \mathbf{u}$ represents the minimum error that affects particles

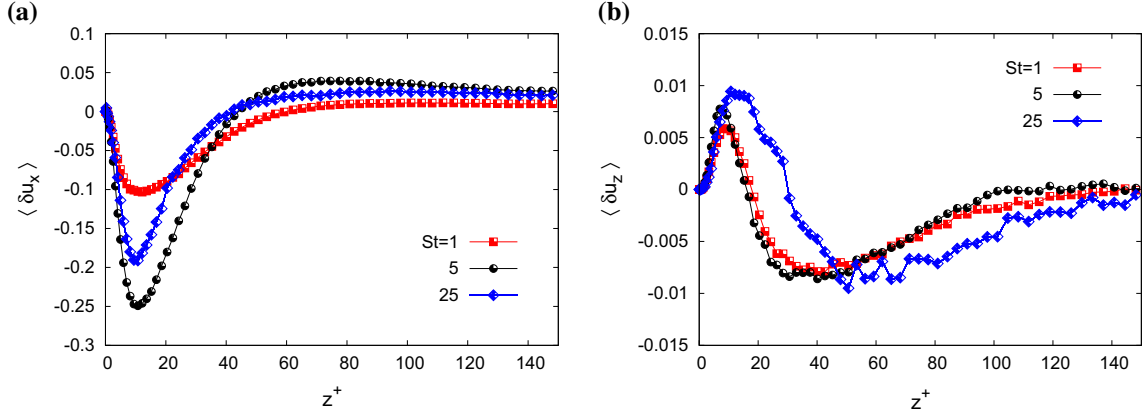


Fig. 9 Mean values of the pure filtering error $\delta \mathbf{u}$ in the streamwise (a) and wall-normal (b) directions at varying particle inertia (parameterized by the Stokes number). Profiles refer to a priori tests with $CF = 4$ (a cut-off filter is used). Reprinted from [13] with the permission of AIP Publishing

even in the ideal situation in which LES provides the exact dynamics of the resolved scales. Figure 9 shows the mean value of the streamwise (Fig. 9a) and wall-normal (Fig. 9b) components of $\delta \mathbf{u}$, measured along the trajectory of three particle sets with different inertia. It is apparent that the error is significantly different from zero almost everywhere throughout the channel and exhibits a near-wall peak (negative for $\langle \delta u_x \rangle$, positive for $\langle \delta u_z \rangle$), followed by a peak of opposite sign farther from the wall. This complex behaviour can be linked to the filtering effects on the near-wall structures discussed in Fig. 7. It was also shown that the PDFs of $\delta \mathbf{u}$ components are strongly skewed and non-Gaussian [13,23], with little dependence on the Reynolds number and particle inertia [39]. This hints at the inadequacy of linear Langevin-type closures for \mathbf{u}_s , based on linear drift and constant diffusion coefficient.

Other studies [137,140] have examined the effect that filtering has on the Lagrangian integral timescale of the SGS fluid seen by a fluid particle, $T_{L,SGS}$,² and the one seen by an inertial particle, $T_{L,SGS}^{@p}$. These observables are crucial parameters of stochastic particle SGS models, as is discussed in Sect. 3. Investigations have focused on HIT in the absence of gravity, where filtering is found to increase $T_{L,SGS}$. This timescale may become larger than the Eulerian one, $T_{E,SGS}$, even if the Lagrangian integral timescale of the full velocity field, T_L , is smaller than the Eulerian one, T_E . This suggests the importance of relating the limiting values of the timescale seen by an inertial particle $T_{L,SGS}^{@p}$ to $T_{L,SGS}$ and $T_{E,SGS}$ rather than considering T_L and T_E to recover the SGS contributions to particle motion [54]. The closure of $T_{L,SGS}^{@p}$, however, is one of the open modelling issues and may become particularly challenging in the presence of gravitational settling [54].

3 Overview of particle SGS models

As mentioned in the Introduction, the first attempt to model the effects of the subgrid fluid velocity on particle motion was made by Wang and Squires [131], who proposed to compute this velocity using the local subgrid kinetic energy, k_{SGS} . In scalar form:

$$u'_{s,i} = \chi \sqrt{\frac{2}{3} k_{SGS}} \quad (7)$$

where χ is a Gaussian random number with zero mean and unit variance. Since this pioneering work, several classes of particle SGS models have been developed. These models, which are suitable either for LES or RANS or both, can be grouped into two main categories [98,115]: structural models (sometimes referred to as deterministic [21]), which aim at reconstructing the entire subfilter velocity field, and stochastic models (sometimes referred to as functional [98]), which aim at retrieving only some statistical features of the subfilter

² The Lagrangian integral timescale of the subgrid fluid velocity seen by a fluid particle is defined as follows: $T_{L,SGS} = \int_0^\infty R_{L,SGS}(\tau) d\tau$, where $R_{L,SGS}(\tau) = \frac{\langle u'_{f,i}(\mathbf{x}_{fp}(t_0), t_0) u'_{f,i}(\mathbf{x}_{fp}(t_0+\tau), t_0+\tau) \rangle}{\langle u'_{f,i}(\mathbf{x}_{fp}(t_0), t_0) u'_{f,i}(\mathbf{x}_{fp}(t_0), t_0) \rangle}$ is the subgrid fluid velocity correlation seen by a fluid particle along its trajectory \mathbf{x}_{fp} .

velocity field. In the following, the most common models belonging to either of these two categories are presented. We remark here that almost all available models refer to the so-called dilute regime, in which the volume fraction and the mass fraction of the dispersed phase are low enough to neglect particle-induced changes in the momentum of the fluid and particle–particle interactions. In the dilute regime, only the fluid turbulence is affecting particle motion, and a one-way coupling between the phases holds. Up to now, no particle SGS models have been developed for semi-dilute or dense suspensions, which would require specific source terms to account for two-way coupling (inter-phase momentum exchange) or four-way coupling (collisions) in the governing equations. In two-way coupled simulations, the typical approach is to use an approximation for the extra terms that appear in the transport equation of k_{SGS} due to the reaction force by which the momentum transfer from the particles to the fluid is modelled (e.g. in the force coupling model [126]). In addition, models apply to point-particle simulations only: Fully resolved simulations, which are the alternative numerical approach to particle-laden flows (in particular, for the simulation of finite-size particles [9]), do not require any kind of closure as they resolve the fine-scale details of the flow around each particle and hence provide a complete description of the hydrodynamic interactions between the particle and the surrounding fluid.

3.1 Structural models

Structural models are developed to provide an approximate reconstruction of the subgrid scales of the flow field. Compared to stochastic models, the main advantage is therefore the capability to reintroduce the effect of such scales on two-point spatial correlations, which in turn control important phenomena such as relative particle dispersion, collisions, break-up and coalescence [120, 124].

3.1.1 Approximate deconvolution (ADM)

The basic idea behind this approach is to obtain an approximate deconvolved velocity field, indicated as $\mathbf{u}^*(\mathbf{x}_p, t)$ hereinafter, by applying a suitably defined filter kernel G to the filtered flow field provided by LES, $\bar{\mathbf{u}}(\mathbf{x}_p, t)$ [1, 2]. If the filter kernel is invertible, then the regularized inverse operator can be approximated by a van Cittert series truncation [123]:

$$G^{-1} \simeq \sum_{n=0}^N (I - G)^n \quad (8)$$

where I is the identity operator and N is the truncation parameter (the most common value found in the literature is $N = 5$ [123]). Using Eq. (8), the deconvolved velocities can be obtained by consecutively applying the filter [117]:

$$u_i^* = \sum_{n=0}^N (1 - G)^n * \bar{u}_i = \bar{u}_i + (\bar{u}_i - \bar{\bar{u}}_i) + (\bar{u}_i - 2\bar{\bar{u}}_i + \bar{\bar{\bar{u}}}_i) + \dots \quad (9)$$

ADM allows partial recovery of the subgrid kinetic energy by enhancing scales near the cut-off by mimicking the behaviour of a sharp spectral filter: Because of this, however, ADM cannot recover energy contributions associated with scales smaller than the filter size. Kuerten [62] was the first to use ADM as subgrid closure for the equations of particle motion, followed by Shotorban and Mashayek [117, 118] and Marchioli et al. [72]. For the same flow configuration (turbulent channel flow at shear Reynolds number $Re_\tau = 150$, based on the half channel height), these authors reported a significant improvement in some statistics of \mathbf{u}_s (in particular the root mean square of fluid velocity components) but less satisfactory predictions in terms of preferential concentration and wall accumulation. This can be explained considering that ADM can reconstruct only the fraction of the subgrid velocity field associated with wavenumbers close to the cut-off value Δ^{-1} . Because of this intrinsic limitation of the approach, ADM is expected to perform less well with flows at high Reynolds number: In these flows, where the range of unresolved scales is wider because of coarser grids, larger filter widths and higher cut-off length scales must be used to cope with the increased computational costs of the simulation [62].

A very recent model, also based on the idea of reconstructing the velocity field only at scales larger than the filter size, has been proposed by [89, 90]. This model uses differential filters of elliptic type [41, 42] to compute the components of the deconvolved velocity field as:

$$u_i^* = \bar{u}_i - b^2 \frac{\partial^2 \bar{u}_i}{\partial x_j \partial x_j} \quad (10)$$

where b is the only model parameter, needed to control the nominal filter width. The value of b is determined using a dynamic procedure that imposes consistency between the SGS energy dissipation calculated from the subgrid model adopted for the fluid stress tensor (the dynamic Smagorinsky model in [89,90]) and the SGS dissipation yielded by the differential-filter model for the particles. Among the possible quantities to be matched, energy dissipation was chosen to ensure correct prediction of the rate at which energy is transferred from the resolved to the subgrid scales, which is crucial for the successful performance of dynamic subgrid models [89,90]. In Sect. 4, application of such model to incompressible HIT is discussed.

3.1.2 Fractal interpolation (FI)

FI has been applied as structural model of subgrid particle dispersion [73]. The basic idea behind the closure hypothesis is to reconstruct the velocity field \mathbf{u} from the filtered field $\bar{\mathbf{u}}$ at scales smaller than the LES filter size, namely at wavenumbers higher than k_c in Fig. 5a. This is done by iteratively applying an affine mapping procedure to $\bar{\mathbf{u}}$, which is available on the coarse-grained LES grid, to reconstruct the velocity signal on a finer DNS-like grid based on the fractal dimension of the signal (which must be known or assumed a priori: We refer to [73,114] for more details). For a 1D signal available at discrete nodes in the interval $[x_{i-1}, x_{i+1}]$, the mapping is defined as follows:

$$W_i[u](\xi) = d_1 \cdot \bar{u}(2 \cdot \xi) + q_{i,1}(2 \cdot \xi) \quad \text{for } \xi \in \left[0, \frac{1}{2}\right], \quad (11)$$

$$W_i[u](\xi) = d_2 \cdot \bar{u}(2 \cdot \xi - 1) + q_{i,2}(2 \cdot \xi - 1) \quad \text{for } \xi \in \left[\frac{1}{2}, 1\right] \quad (12)$$

where $\xi = (x - x_{i-1})/2\Delta$ is a dimensionless coordinate normalized by the grid spacing $\Delta = (x_{i-1} - x_{i+1})/2$, and:

$$q_{i,1}(\xi) = [\bar{u}_i - \bar{u}_{i-1} - d_1 \cdot (\bar{u}_{i+1} - \bar{u}_{i-1})] \cdot \xi + \bar{u}_{i-1} \cdot (1 - d_1), \quad (13)$$

$$q_{i,2}(\xi) = [\bar{u}_{i+1} - \bar{u}_i - d_2 \cdot (\bar{u}_{i+1} - \bar{u}_{i-1})] \cdot \xi + \bar{u}_i - d_2 \cdot \bar{u}_{i-1}. \quad (14)$$

The characteristics of the reconstructed signal depend on the two stretching parameters, d_1 and d_2 , which in turn depend on the fractal dimension of the signal. In HIT (see [114]), these parameters are typically assumed constant in time and uniform in space, and set to $d_1 = 2^{-1/3}$ and $d_2 = -2^{-1/3}$. This corresponds to a fractal dimension of the velocity signal of 1.7. Algorithms have been developed [109] to compute the stretching parameters locally, using the discrete values on a fine grid (DNS data). These algorithms do not require the a priori knowledge of the fractal dimension of the signal: In wall-bounded flows, locally computed stretching parameters exhibit a noticeable variation in the wall-normal (anisotropy) direction and attain values that are significantly lower than those experimentally obtained in HIT: We refer again to [73] for further details. Indeed, one of the main issues with FI is the estimate of the stretching parameters in non-homogeneous flows, and in particular their behaviour in the near-wall region. Another problem of the method is that it does not guarantee a correct reconstruction of the correlation of different velocity components, needed to correctly retrieve the subgrid stresses (especially in shear flows) [98]. Application of FI to particle-laden turbulent channel flow [73] indicates that FI performs well close to the channel centreline, where turbulence is closer to being homogeneous and isotropic, and particle velocity and concentration statistics can be retrieved with reasonable accuracy.

3.1.3 Kinematic simulation (KS)

KS represents a computationally simple structural approach to model subgrid effects on particles upon representing the small-scale velocity field by means of Fourier modes. Based on a prescribed turbulent kinetic energy spectrum, a subgrid fluid velocity field is generated using a large number of separate random orthogonal Fourier modes with prescribed wavenumbers and frequencies [37]:

$$\mathbf{u} = \sum_{n=1}^{N_k} [\mathbf{a}_n \times \mathbf{k}_n \cos(\mathbf{k}_n \cdot \mathbf{x} + \omega_n t) + \mathbf{b}_n \times \mathbf{k}_n \sin(\mathbf{k}_n \cdot \mathbf{x} + \omega_n t)] \quad (15)$$

where N_k is the number of modes, \mathbf{k}_n represents the wavenumbers, ω_n the frequencies that determine the unsteadiness associated with each wavenumber, and \mathbf{a}_n and \mathbf{b}_n are random coefficients chosen to satisfy the incompressibility constraint $\nabla \cdot \mathbf{u} = 0$. The magnitude of the cross-products $|\mathbf{a}_n \times \mathbf{k}_n|^2 = |\mathbf{b}_n \times \mathbf{k}_n|^2 = E(k_n)\Delta k_n$, where $E(k_n)$ is a prescribed Eulerian energy spectrum (typically $E(k_n) \sim k^{-p}$ with $1 < p < 2$), should yield the prescribed energy spectrum beyond the cut-off wavenumber used in LES. Compared to the simplest stochastic models, which treat the subgrid fluid velocity field as white noise, the advantage of closures based on KS is that the subgrid field can have an underlying structure and turbulent structures that are smaller than the filter size can, in principle, be accounted for. The method is also computationally cheap and contains no arbitrarily adjustable parameters. In spite of these advantages, however, application of KS as SGS model for particles is so far limited to HIT (see e.g. [34, 106]). This is because application of the method to non-homogeneous flows and/or flows with boundary conditions (e.g. wall-bounded flows) involves a number of non-trivial implementation issues regarding the nature of the KS field near the walls and also when the grid resolution becomes comparable to the Kolmogorov scale [98]. This is because the typical approach is to use a zonal LES model in which the strength of the velocity field that KS adds as subgrid contribution to the filtered LES field is controlled by the cut-off energy dissipation from LES, which becomes small near the wall. In this region, the zonal model switches to an RANS model near the wall; thus, the KS is also switched off.

To the best of this author's knowledge, there are only two investigations [59, 106] where KS is applied in combination with LES. In [59], particle deposition in turbulent channel flow (with a ribbed wall) is examined. In this work, the parameters for KS are the energy dissipation rate obtained from LES, the energy spectra, ratio of the largest and smallest subgrid scales, and the total number of modes for the subgrid velocity field. The only free parameter is the power law of the energy spectrum: All the other parameters of the model are fixed by the resolved LES flow field. One crucial open question, however, is when to switch the KS off near the wall. In [106], KS is used to predict clustering and relative velocity statistics in the absence of gravitational settling. Very good agreement against DNS data is found only for relatively large values of the Stokes number based on the Kolmogorov timescale, while the mean inward radial relative velocity (important because it is used in the collision kernel) is well predicted for all Stokes numbers investigated.

3.1.4 Spectrally optimized interpolation (SOI)

SOI is a rather unique particle SGS model, proposed by Gobert and Manhart [44]. SOI tries to model the subgrid fluid velocity by exploiting a specific interpolation method that extends approximate deconvolution towards higher wavenumbers. The idea is similar to using implicit LES as a fluid SGS model: In SOI, fluid velocity interpolation is optimized such that the particles see a prescribed energy spectrum, which has to be correctly represented all the way down to the Kolmogorov scales. By doing so, SOI goes beyond ADM, as Gobert and Manhart verified for the case of particle-laden forced HIT [44]. The computational costs for SOI are comparable to fourth order interpolation. The model has been developed (and tested) only in the framework of homogeneous isotropic turbulence, even if extensions to arbitrary flow are possible (e.g. using wavelets as a substitute for the Fourier transforms to provide a localized decomposition of the flow field into its scales [11, 44] and compute the SOI stencil on a local basis [44]). It must be noted that SOI requires availability of a model spectrum, which is usually unknown a priori in inhomogeneous anisotropic turbulent flows.

3.2 Stochastic models

Stochastic models are typically based on a Lagrangian diffusion-type equation for the subgrid fluid velocity. The formulation of such an equation is made in analogy with single-phase turbulence closures that model the impact of subgrid scales on the resolved ones by means of an additional viscosity [98]. These models have been widely employed to predict particle deposition and resuspension, especially in the context of Reynolds-averaged formulations for industrial applications [83, 85, 102]. Over the last decade, however, growing efforts have been devoted to the extension of stochastic closures to LES with subgrid modelling [60, 61, 82–85]. From an historical perspective, stochastic models were initially developed for free-shear flows in the context of environmental fluid mechanics [98], and closures were typically formulated for the fluid velocity seen by the particles along their trajectory (referred to as velocity seen hereinafter). There is a wide literature on the subject for RANS, and we refer to [24, 85, 86, 91] for a comprehensive review and critical analysis. In the following, we focus on SGS models specifically developed for LES.

The first formulations were developed for the particle velocity itself, one early example being the stochastic closure by Fukagata et al. [36]. These authors proposed to account for subgrid turbulence effects on particle

motion by adding a subgrid Brownian force on the right-hand side of Eq. (1). This term is defined as:

$$\frac{F_{SGS}}{m_p} = \frac{\sigma_s}{\Delta t} \xi \quad (16)$$

where $\sigma_s = \sqrt{2k_{SGS}\lambda/3}$ is the increase in standard deviation of particle velocity due to SGS velocity, fluctuations during the simulation time step Δt (the parameter λ is a complicated function of τ_p and τ_{SGS}), and ξ is a Gaussian random number with zero mean and unit variance. All subgrid contributions to Eq. (1) are included in this force term: Other forces (e.g. drag) are computed using the filtered fluid velocity. The model of Fukagata et al. [36] was later improved by Amiri et al. [5] to account for flow anisotropy by the use of damping functions. Another Brownian-like model was later proposed by Bini and Jones [14, 15], who introduced nonlinearity in the subgrid force term to account for the far-from-Gaussian behaviour of particle acceleration demonstrated by experiments [64, 65]. The model was used to study turbulent sprays, focusing in particular on droplet SGS dispersion statistics.

The most widely used Lagrangian stochastic approaches, however, deal with the modelling of the fluid velocity seen, which determines the pure filtering error affecting the estimation of the forces acting on particles in LES. The starting point of these approaches is represented by the following Langevin type of closure:

$$d\mathbf{u}_s = \underbrace{\mathbf{A}dt}_{\text{deterministic term}} + \underbrace{\mathbf{B}d\mathbf{W}}_{\text{stochastic term}} \quad (17)$$

where \mathbf{A} and \mathbf{B} represent suitably parameterized drift (deterministic) and diffusion (stochastic) matrices, respectively, whereas $d\mathbf{W}$ is the vector of independent increments of a Wiener process. In the simplest formulation, these increments are Gaussian random variables with zero mean and variance dt .

Several closures for \mathbf{u}_s , or alternatively for its subgrid part \mathbf{u}'_s , have been proposed and tested in both homogeneous isotropic turbulence (more often) and wall-bounded turbulence [12, 31, 32, 98, 100, 116]. One of the first closures was proposed by Pozorski and co-workers (see [100]), based on the following stochastic differential equation of the Ito type:

$$d\mathbf{u}'_s = -\frac{\mathbf{u}'_s}{\tau_{SGS}} dt + \sqrt{\frac{2\sigma_{SGS}^2}{\tau_{SGS}}} d\mathbf{W} \quad (18)$$

where $\sigma_{SGS} = \sqrt{2k_{SGS}/3}$ is the subgrid velocity scale obtained from the kinetic energy of the non-resolved flow scales k_{SGS} , and $\tau_{SGS} = C_{SGS}\Delta/\sigma_{SGS}$ is the subgrid timescale based on the model constant C_{SGS} and on the filter width Δ . In filtered DNS (referred to as *a priori* LES hereinafter), k_{SGS} is known. In true LES (referred to as *a posteriori* LES hereinafter), k_{SGS} must be estimated. Pozorski and Apte [100] proposed the following expression:

$$k_{SGS} = C_I \bar{\Delta} |\bar{S}|^2 \quad (19)$$

where the parameter C_I can be found from the dynamic Germano procedure with double filtering [40] and $|\bar{S}| = (2\bar{S}_{ij}\bar{S}_{ij})^{1/2}$ is the magnitude of the resolved strain rate based on the second invariant of $\bar{S}_{ij} = (\partial\bar{u}_i/\partial x_j + \partial\bar{u}_j/\partial x_i)/2$.

This model was later improved based on an exact formulation for the deterministic terms, by analogy to turbulent dispersion in RANS. In particular, Shotorban and Mashayek [116] and Fede et al. [32] proposed a model for the subgrid fluid velocity seen along the trajectory of a fluid parcel, which appears to work reasonably well also for particles with very low inertia. Both models account for the spatial inhomogeneity of the fluid velocity statistics in LES and are based on the following general equation:

$$d\mathbf{u}'_s = [-(\mathbf{u}' \cdot \nabla)\bar{\mathbf{u}} + \nabla \cdot \boldsymbol{\tau}'] dt + \mathbf{G}_{fp} \mathbf{u}'_s dt + \mathbf{B}d\mathbf{W} \quad (20)$$

where $\boldsymbol{\tau}'$ is the subgrid scale stress tensor, \mathbf{G}_{fp} is a second-order tensor that has physical dimensions of a frequency and whose elements are closed as $G_{fp,ij} = -\delta_{ij}/T_{L,SGS}^{\text{@}p} = -\delta_{ij}/T_{L,SGS}$ with δ_{ij} the Kronecker delta. Note that the subgrid Lagrangian integral timescale $T_{L,SGS}^{\text{@}p}$ is assumed to be equal to $T_{L,SGS}$, this being true only in the limit $St \ll 1$. The diffusion matrix is defined as $\mathbf{B} = \sqrt{C_0\epsilon_{SGS}}$, where C_0 is the Kolmogorov constant, and:

$$\epsilon_{SGS} = \nu \frac{\partial u_{s,i}}{\partial x_j} \frac{\partial u_{s,j}}{\partial x_i} \quad (21)$$

is the subgrid fluid velocity dissipation. The closure adopted for $T_{L,SGS}$ and for ϵ_{SGS} read:

$$T_{L,SGS} = \left[\frac{1}{2} + \frac{3C_0}{4} \right]^{-1} \frac{k_{SGS}}{\epsilon_{SGS}}, \quad (22)$$

$$\epsilon_{SGS} = C_S \Delta^2 |\bar{S}|^3, \quad (23)$$

with $k_{SGS} = 2C_Y \Delta^2 |\bar{S}|^2$, where C_S and C_Y are the Smagorinsky and Yoshizawa constants, respectively [119, 141]. The model just presented was developed for particles with relaxation time close to the subgrid timescale of fluid turbulence and ensures that the equation for the variance of the subgrid fluid velocity along particle trajectory is consistent with the mean subgrid kinetic energy equation that is obtained from the filtered Navier–Stokes equations.

This model was later extended to wall-bounded flows by Knorps and Pozorski [60], who proposed the following expression for the diffusion matrix to account for the correlation among the subgrid fluid velocities:

$$\mathbf{B} = \sqrt{\frac{2}{T_{L,SGS}^{\textcircled{p}}}} \begin{bmatrix} \sqrt{\left(\overline{u_x'^2} - \overline{u_x' u_y'}^2 / \overline{u_y'^2} \right)} & 0 & 0 \\ \overline{u_x' u_y'} / \sqrt{\overline{u_x'^2}} & \sqrt{\overline{u_y'^2}} & 0 \\ 0 & 0 & \sqrt{\overline{u_y'^2}} \end{bmatrix} \quad (24)$$

where $\overline{u_i'^2}$ and $\overline{u_i' u_j'}$ are the variances and covariances of the subgrid velocities, respectively. Such velocity correlations are computed using a generalized Yoshizawa-like formula in which a wider filter is applied on top of the LES filter [99]. To avoid unphysical nonzero values of the subgrid timescale at the wall, a van Driest damping is adopted:

$$T_{L,SGS}^{\textcircled{p}} = [1 - \exp(-y^+/25)] C_{SGS} \bar{\Delta} / \sqrt{2k_{SGS}/3} \quad (25)$$

where C_{SGS} is a user-chosen constant that can be adjusted depending on the particle relaxation time [98]. Such dependence, however, is non-trivial and still constitutes one of the main issues in stochastic modelling.

There are several other formulations available in the open literature (see e.g. [3, 12, 92, 126, 127]), which are also based on Eq. (20) but adopt different correlations for the timescale τ_{SGS} and for the diffusion term constant C_0 . In particular, the model by Berrouk et al. [12] solves for Eq. (20) replacing \mathbf{u}'_s with \mathbf{u}_s :

$$d\mathbf{u}_s = \left(-\frac{\nabla p}{\rho} + \frac{1}{Re} \nabla^2 \bar{\mathbf{u}}_f \right) dt - \left(\frac{\mathbf{u}_s - \bar{\mathbf{u}}_f}{T_{L,SGS}^{\textcircled{p}}} \right) dt + \sqrt{C_0^* \langle \epsilon_{SGS} \rangle} d\mathbf{W}, \quad (26)$$

assuming the following dependence of $T_{L,SGS}^{\textcircled{p}}$ on particle inertia [133]:

$$T_{L,SGS}^{\textcircled{p}} = \frac{T_{L,SGS}}{\beta} \left[1 - (1 - \beta)(1 + St_{E,SGS})^{-0.4(1+0.01St_{E,SGS})} \right] \frac{1}{b_i} \quad (27)$$

where $T_{L,SGS}$ is the Lagrangian SGS timescale of the fluid, $\beta = T_{L,SGS}/T_{E,SGS}$ is the ratio of the Lagrangian and Eulerian ($T_{E,SGS}$) SGS timescales of the fluid, $St_{E,SGS} = \tau_p/T_{E,SGS}$ is the Stokes number based on $T_{E,SGS}$, and b_i are the so-called Csanady factors, which are used to account for the crossing trajectory and continuity effects [3, 25, 135, 142].

When the reference system is aligned with the mean, or filtered, slip velocity, the Csanady factors can be defined as (see [83, 86] for details):

$$b_i = \begin{cases} b_{\parallel} = \sqrt{1 + \beta^2 \frac{|\langle u_r \rangle|^2}{\frac{2}{3} \langle k_{SGS} \rangle}}, \\ b_{\perp} = \sqrt{1 + 4\beta^2 \frac{|\langle u_r \rangle|^2}{\frac{2}{3} \langle k_{SGS} \rangle}}, \end{cases} \quad (28)$$

with subscripts \parallel and \perp representing the mean drift and transverse directions, respectively, whereas $\langle u_r \rangle$ is the mean relative velocity between the particle and the fluid seen. Equation (27) exhibits the correct asymptotic

behaviour for particles with very small inertia, for which $T_{L,SGS}^{\textcircled{p}} \simeq T_{L,SGS}$, and for particles with very high inertia, for which $T_{L,SGS}^{\textcircled{p}} \simeq T_{E,SGS}$ [54]. The closure adopted for the diffusion term constant reads as:

$$C_0^* = C_0 b_i \frac{\hat{k}_{SGS}}{k_{SGS}} + \frac{2}{3} \left(b_i \frac{\hat{k}_{SGS}}{k_{SGS}} - 1 \right) \quad (29)$$

where \hat{k}_{SGS} is a modified subgrid kinetic energy that is weighted by the Csanady factors to account for anisotropy: Hence $\hat{k}_{SGS}/k_{SGS} = 1$ in homogeneous isotropic flows. The model by Berrouk et al. [12] is similar to the model by Pozorski and Apte [100], since both account for the crossing trajectory and continuity effects [25,135]. In a recent work, Cernick et al. [21] have assessed the performance of different stochastic models (those proposed by Fukagata et al. [36], Shtorban and Mashayek [116], Berrouk et al. [12]) for the case of inertial particles in decaying HIT, upon comparison against DNS results with and without gravity. Stochastic models generally performed well at small Stokes numbers and were able to recover the correct amount of subgrid energy removed by LES filtering. However, models were unable to predict preferential concentrations and showed strong sensitivity to the Stokes number and filter size (see Sect. 4 for a more detailed discussion). Vinkovic et al. [126,127] also employed a stochastic particle SGS model based on a modified Langevin equation written in terms of the local SGS characteristics and on a Lagrangian correlation timescale chosen ad hoc to include the influence of gravity and particle inertia. This model was used to study atmospheric dispersion of sediments [126] and pollutants [127,134].

The models described so far aim at reconstructing the subgrid fluid velocity seen or the *full* fluid velocity seen. However, formulations for the fluid acceleration can also be derived. To the best of this author's knowledge, the only formulation available for the fluid acceleration has been first proposed by Sabel'nikov et al. [111] and later applied by Zamansky et al. [143] to study acceleration statistics in turbulent channel flow.

4 Example of applications

The modelling issue that is most relevant to the present review is whether particle SGS models can capture preferential concentration and, in turn, all the physical processes that it produces (in particular, clustering as well as near-wall accumulation and segregation). To address this issue, a number of different testing configurations and governing parameters have been considered, which make it difficult to compare the relative performance of different particle SGS models. In the following, an overview of recent findings is provided considering three main instances: spherical particles in homogeneous isotropic turbulence, spherical particles in wall-bounded flow and non-spherical particles in homogeneous isotropic turbulence.

4.1 Spherical particles in homogeneous isotropic turbulence

Most of the studies dealing with particle-laden flows in LES consider the situation in which sub-Kolmogorov spherical particles are dispersed in homogeneous isotropic turbulent flow. Among these studies, Gobert and Manhart [45] have compared ADM [62] against two stochastic models [32,117] performing both a priori and a posteriori tests in HIT (at $Re_\lambda = 52$, and for Kolmogorov-based Stokes numbers ranging from 0.1 to 100). Based on the statistics of fluid kinetic energy seen, particle kinetic energy and dispersion rate, it was found that the stochastic model performs poorly compared to ADM, especially at high Stokes numbers. However, the good predictions of ADM are expected to get worse at much higher Reynolds numbers, when the LES grid inevitably becomes more coarse-grained to cope with computational costs and the range of unresolved scales (where ADM cannot reconstruct the filtered fluctuations) widens. Building on this comparison, criteria for model selection and reliability prediction were later provided, based on an analytical estimate for the model error in dependence of the particle Stokes number and of the energy spectrum of the flow [46].

The same flow configuration has been considered by Cernick et al. [21] to assess the ability of the particle SGS model to predict preferential concentration. Assessment is based on the quantification of the fractal dimension d_{pc} of particle clusters. This observable provides a measure of the spatial distribution of particle distribution and is defined as the slope of the $N_p(r_i)$ curve, N_p being the number of particles within a sphere of radius r_i centred around a base particle. A fractal dimension $d_{pc} = 3$ corresponds to a perfectly random

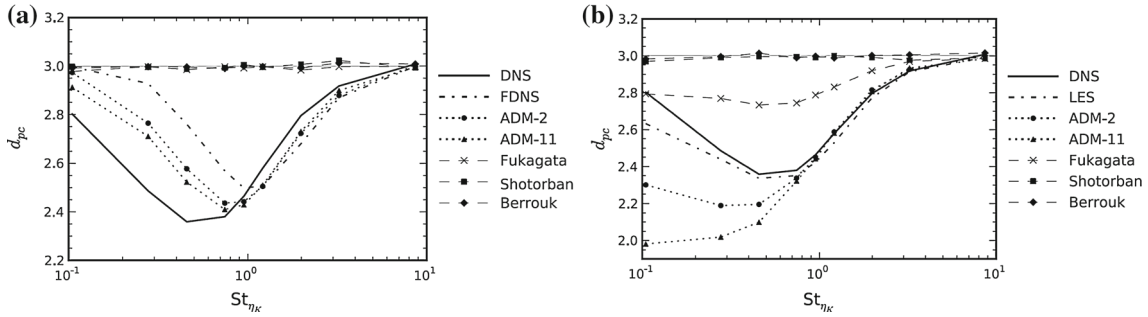


Fig. 10 Fractal dimension of particle clusters in homogeneous isotropic turbulence. **a** a priori tests with coarsening factor $CF = 8$ ($\Delta = 8\Delta_{DNS}$) and **b** a posteriori tests with $CF = 16$. Reprinted from [21]

distribution of particles, whereas lower values indicate clustering (over a surface if $d_{pc} = 2$ or along a line-like structure if $d_{pc} = 1$): The smaller the value of d_{pc} , the larger the degree of preferential concentration. In Fig. 10, the behaviour of d_{pc} as a function of the Kolmogorov-based Stokes number St_K is shown for inertial particles of different sizes in decaying incompressible HIT (and in the absence of gravity). The solid line refers to DNS results, the dashed line refers to filtered DNS (FDNS, a priori testing) in panel (a) and to LES (a posteriori testing) in panel (b); symbols refer to results yielded by four different particles SGS models: Approximate deconvolution (ADM) and the stochastic models of Fukagata et al. [36], Shotorban [116] and Berrouk et al. [12] presented in Sect. 3.2. For the Reynolds number considered by [21] ($Re_\lambda = 74$ based on the Taylor microscale), the minimum value of d_{pc} in DNS is slightly below 2.4 at $St_K \simeq 0.5$. As already discussed in Sect. 2, filtering reduces (increases) clustering at small (large) Stokes numbers [72, 107]. Let us focus first on Fig. 10a. Compared to FDNS, results for approximate deconvolution (ADM-2 being relative to a truncation level $N = 2$, ADM-11 being relative to a truncation level $N = 11$) show better agreement with DNS, because this technique can recover the energy associated with the flow scales near the cut-off. However, the degree of clustering is still under-predicted (over-predicted) at low (high) St_K because particle motion is anyhow affected by the subgrid scales, whose energy cannot be recovered by ADM: Clustering of small particles is reduced because filtering removes precisely the subgrid eddies that control preferential concentration of such particles; clustering of large particles is increased because they do not experience the long-term randomizing effect of the subgrid eddies [31, 107]. The three stochastic models are found to predict no clustering regardless of the Stokes number: This is ascribed to the random component of the models, which appears to act as strong mixing agent that overwhelms the effect of the resolved flow structures on particle distribution in the a priori tests. Focusing now on Fig. 10b, it can be observed that LES results are similar to the FDNS ones at the large scales, whereas the higher amount of energy that is typically associated with the smallest resolved scales in LES with respect to FDNS determines a significant increase in preferential concentration of the small- and intermediate-inertia particles. This trend is further emphasized with ADM, which adds energy precisely to the scales near the cut-off and leads to reduced particle dispersion. Similar results have been obtained in [44]. As far as the stochastic models are concerned, only the model of Fukagata et al. [36] predicts some degree of clustering but this is due to the specific formulation used to calculate the SGS turbulent kinetic energy of the fluid rather than to a direct effect of the particle SGS model. Overall, the analysis of Cernik et al. [21] indicates that standard stochastic particle SGS models cannot capture particle–turbulence interactions properly.

Park et al. [89, 90] have applied their differential-filter (DF) model (described in Sect. 3.1.1) to simulate the dispersion of sub-Kolmogorov particles in dilute HIT at $Re_\lambda = 85$. Results from a posteriori LES on a 32^3 grid have been compared with DNS ones on a 256^3 grid. In this review, we show the particle concentration spectra for particles with increasing inertia, parameterized here by the Stokes number based on the Kolmogorov timescale St_K , as a function of the dimensionless wavenumber kl_k where l_k is the Kolmogorov length scale. Compared to the reference DNS statistics, the improvement of preferential concentration granted by the dynamic DF model is evident for $St_K < 1$ and $St_K > 1$, especially in the energetic part of the concentration spectra. This results from the capability of the model to predict the non-monotonicity of particle preferential concentration at increasing particle inertia (not shown). However, the DF model underperforms when St_K is around unity: The reasons for such inferior performance are not yet clear and are currently under investigation (Fig. 11).

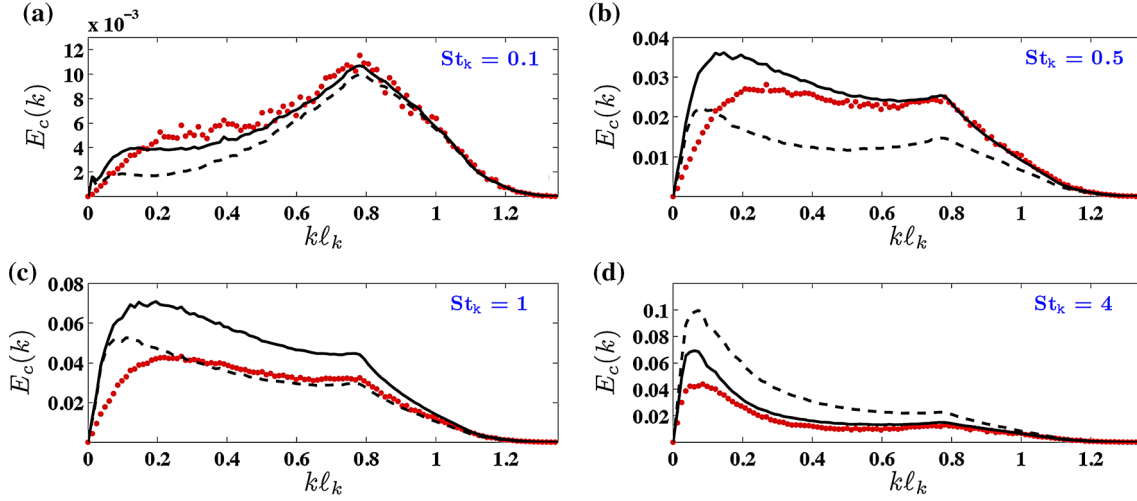


Fig. 11 Particle concentration spectra as functions of the dimensionless wavenumber, kl_k , in homogeneous isotropic turbulence at varying particle Stokes number based on the Kolmogorov timescale, St_K . **a** $St_K = 0.1$, **b** $St_K = 0.5$, **c** $St_K = 1$, **d** $St_K = 4$. Lines and symbols DNS (circles), LES without particle model (dashed lines), LES with DF model (solid lines). Reprinted from [89,90] with permission from the authors

4.2 Spherical particles in wall-bounded turbulence

Applications of particle SGS models to wall-bounded turbulence are more recent and focus mainly on channel flow configurations. Breuer and Happe [17] tested the influence of the Langevin SGS model of Pozorski and Apte [100], extended for an arbitrary direction of particle motion [85], to bubble-laden and particle-laden turbulent channel flow. In the bubble-laden case, a well-resolved LES was performed, and therefore, the SGS model was found to yield subgrid velocities of small magnitude: Only marginal changes in both the velocity statistics and the volume fraction could be observed. The fine grid resolution, however, did not prevent the model from exhibiting a clear influence on particle velocity and concentration statistics in the particle-laden case, where particles with Stokes number $St = 0.1, 1$, and 1.67 were considered: Higher particle volume fractions were obtained at the wall, with a consequent increase in particle-wall and particle-particle collisions that in turn may influence potential deposition and agglomeration processes.

Hybrid models combining structural and stochastic models have also been applied in the literature. Michałek et al. [81] used jointly ADM (for the resolved scales) and a stochastic process of the diffusive type (for the subgrid scales) to study dilute channel flow at different Reynolds numbers (up to $Re_\tau = 950$). The idea is to exploit deconvolution of the filtered fluid velocity field to recover energy up to the smallest resolved scale. Fine tuning of the predicted particle wall-ward fluxes was achieved by including an additional term in the stochastic model to satisfy the well-mixed condition at small Stokes numbers: This term was derived upon direct comparison with DNS results at varying Stokes number and has the form $f(St) = \exp(-St/2)$. The results thus obtained for particle concentration and velocity statistics (especially the mean wall-normal velocity, which is crucial for predicting turbophoresis) are in good agreement with those of DNS. In addition, the model parameters exhibit weak dependence on the Reynolds number. One interesting feature of the model is that it can be extended quite straightforwardly to include two-way coupling effects at higher particle volume fractions. There are however open issues concerning the parameterization of the Stokes number dependence of the weight factor $f(St)$ that is inherent in the model.

An interesting application of the stochastic particle SGS model (named stochastic subgrid acceleration model—SSAM) has been presented recently by Zamansky et al. [143]. The main feature of this model, which is the product of two independent stochastic processes (one for the acceleration modulus and one for the acceleration orientation) [143], is its capability to reconstruct the instantaneous unfiltered velocity field at the scale of the particle: Therefore, it does not require additional modelling in Eq. (1). Figure 12 shows the model performance in turbulent channel flow for two statistical observables that are directly linked to turbophoresis and preferential concentration: The wall-normal component of particle velocity rms (indicated as v_p^+ in Fig. 12a) and instantaneous particle concentration (indicated as C in Fig. 12b). Note that y^+ represents the wall-normal coordinate in wall units. The improvement granted by SSAM is apparent especially at small Stokes

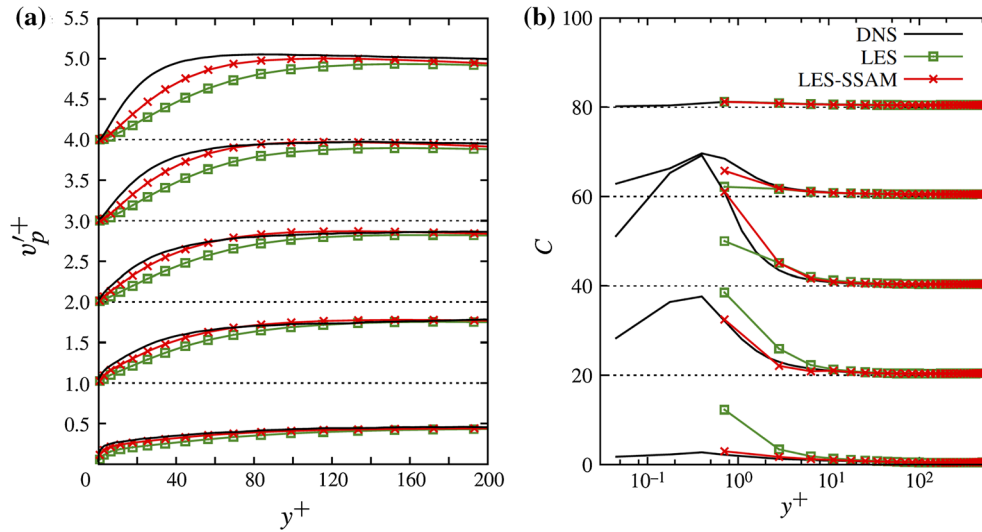


Fig. 12 Comparative assessment of the LES-SSAM model [143] in particle-laden turbulent channel flow ($Re_\tau = 590$): Prediction of the particle wall-normal velocity rms (a) and of particle concentration (b) at varying Stokes number: $St = 1, 5, 15, 25$ and 125 from top to bottom in each panel. *Line* DNS, *squares* LES with no particle SGS model, *crosses* LES with SSAM. All variables are expressed in wall units. Reprinted from [143]

numbers, even if velocity fluctuations are not completely recovered with respect to DNS. However, this is sufficient to obtain quite good agreement with DNS in terms of wall-normal concentration. Note that, as the Stokes number is increased, the concentration profiles for LES without particle SGS model overshoot DNS profiles even if fluctuations along y^+ are damped. Indeed, depending on the specific choice of the particle SGS model, flow configuration and range of Reynolds and Stokes numbers, quite different results can be obtained. Sometimes with better performance by stochastic models, some other times by structural models. Among the latter ones, fractal interpolation is in principle very attractive because of its capability to reconstruct the subgrid part of the flow field by extrapolating scales of the coarse-grained LES field to smaller and smaller scales [73]. This feature should be particularly effective at high Reynolds numbers. Up to now, however, fractal interpolation has been assessed only at low Reynolds numbers, in situations where the velocity signals vary rather smoothly over the LES grid: This makes the interpolation procedure inefficient (there is no fractal form to be copied), and no significant improvement in the prediction of particle statistics and concentration has been observed. An example of such poor behaviour is shown in Fig. 13 [73].

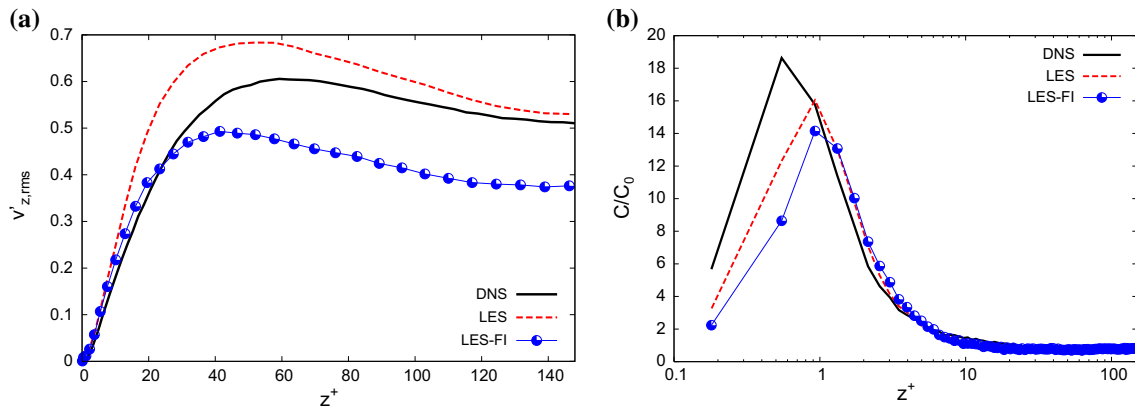


Fig. 13 Comparative assessment of particle SGS model based on fractal interpolation [73] in particle-laden turbulent channel flow ($Re_\tau = 150$): Prediction of the particle wall-normal velocity rms (a) and of particle concentration (b) for Stokes number $St = 5$. *Solid line* DNS, *dashed line* LES with no particle SGS model, *symbols* LES with fractal interpolation. All variables are expressed in wall units. Reprinted from [73]

4.3 Elongated particles in homogeneous isotropic turbulence

All results shown so far are relative to spherical particles. However, there is a growing interest in studying the dynamics of non-spherical particles in turbulent flow because of the central role played in a wide range of engineering applications and environmental problems. The reader is referred to [129] for a review on the subject, which is particularly rich in physics and intriguing from a modelling point of view since particle anisotropy adds to flow anisotropy: The resulting translational and rotational dynamics change significantly with respect to spherical particles. Most of the numerical simulations performed so far are based on DNS of turbulence, but LES is becoming more and more attractive in view of the continuous improvements in the SGS models for both the fluid and the particles. In particular, a recent application of LES to non-spherical particles in the EL framework has been presented by Chen et al. [22]. These authors have considered the effect of including a subgrid closure in the equation of motion of small ellipsoidal particles evolving in HIT and have quantified this effect in terms of particle alignment within the flow and particle orientational distribution. Ellipsoidal particles move according to an equation similar to Eq. (1), in which only the drag force model changes to account for the dependence of the drag coefficient on particle orientation, and rotate according to the well-known Jeffery equation [52]. This equation provides the time evolution of the orientation of an axisymmetric particle, given by the unit vector \mathbf{p} aligned with major symmetry axis, with respect to the velocity gradient tensor seen by the particle:

$$\dot{\mathbf{p}} = \frac{1}{2}\omega \wedge \mathbf{p} + \frac{\alpha^2 - 1}{\alpha^2 + 1} \left(S[\mathbf{u}_s]\mathbf{p} - (\mathbf{p}^T S[\mathbf{u}_s]\mathbf{p})\mathbf{p} \right) \quad (30)$$

where ω is the fluid vorticity along the particle axis, $S[\mathbf{u}_s]$ is the strain-rate tensor (symmetric part of the velocity gradient tensor), and α is the particle aspect ratio. The last term in Eq. (30) is the contribution parallel to \mathbf{p} needed to keep the strain from changing the magnitude of \mathbf{p} . It is natural to expect significant errors in the calculation of \mathbf{p} over time when the exact velocity gradients (available in DNS) are replaced with those computed from the resolved velocity field yielded by LES. In addition, SGS effects are expected also on the rotational dispersion coefficient of the particles: This coefficient depends on the turbulent energy dissipation rate, which is reduced when SGS velocity fluctuations are not accounted for [22]. Indeed, results from a priori tests demonstrate that SGS fluctuations mostly affect particle rotation, resulting in weaker particle alignment with the vorticity field and reduced particle rotational energy if neglected. To recover these effects, both a stochastic SGS model and a model based on ADM have been tested. It should be noted that adopting a stochastic closure for the fluid velocity seen (which typically involves a Wiener process with uncorrelated independent increments and continuous trajectories that are nowhere differentiable) would yield a velocity field that is non-differentiable and velocity gradients would be unavailable: Therefore, a Lagrangian stochastic model for the SGS velocity gradient tensor seen by the particles was adopted (details about this model can be found in [22] and references therein). An example of the performance of the different models is shown in Fig. 14, where particle orientation within the flow is quantified by means of two observables.

One observable is particle alignment with the vorticity field, computed correlating the orientation vector \mathbf{p} to the unit direction vector \mathbf{e}_ω of vorticity, and plotted for the case of ellipsoidal particles with aspect ratio $\alpha = 100$, representing rod-like particles (Fig. 14a). The other is particle mean square rotation rate, $\langle \dot{p}_i \dot{p}_i \rangle$, evaluated over a wide range of aspect ratios, including disc-like particles with $\alpha < 1$ (Fig. 14b). Direct comparison against DNS results shows that the stochastic model (LES-SDE) provides poor prediction of particle alignment and over-prediction (under-prediction) of the reconstructed rotational energy at large (small) aspect ratios. This is probably due to the fact that the stochastic part of the model used by [22] is Gaussian and uncorrelated in time: Therefore, the model cannot take into account any effect due to the anisotropy of particle rotation dynamics, which are correlated with preferential alignment phenomena, and any effect on particle rotational diffusivity due to the different correlation timescales characterizing the particle angular velocities [75]. The ADM-based model has little influence on particle alignment compared to a priori (FDNS) and a posteriori (LES) results, but improves prediction of the rotational energy for aspect ratios larger than unity: This is ascribed to the capability of ADM to recover fluid enstrophy near the cut-off scale [22]. Overall, the difference between the reference DNS results and the results obtained with or without any of the particle SGS models is either marginal or increased indicating that further work is required to improve model predictions with non-spherical particles. A crucial aspect is represented by the choice of the particle state vector. Limiting the discussion to rigid particles with length below the Kolmogorov scale that evolve according to the Jeffery equation, both particle orientation (or its angular velocity) and the fluid velocity gradients seen by the particle at the centre-of-mass location must be included [82]. However, these are small-scale quantities that are extremely complex to model. In some flow

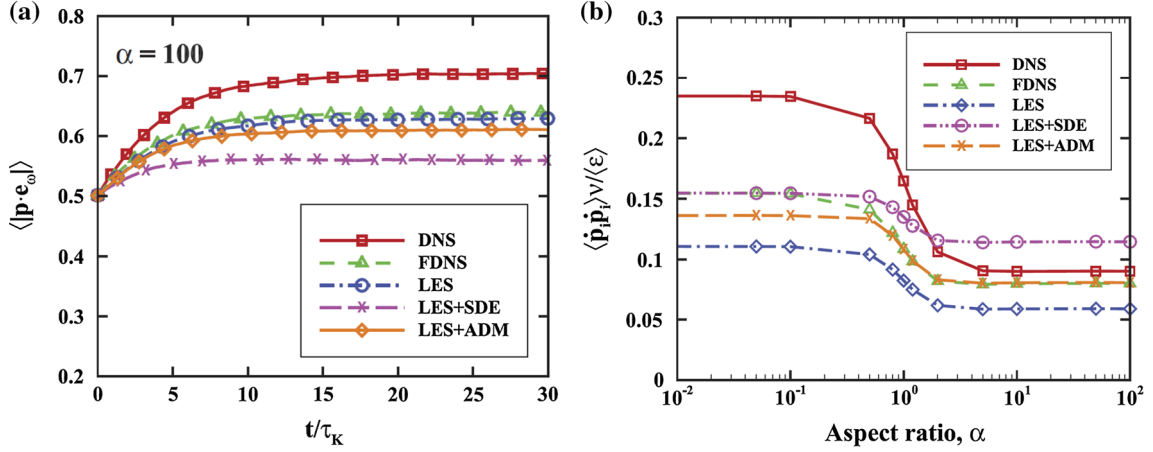


Fig. 14 Comparative assessment of the particle SGS models for ellipsoidal particles in HIT ($Re_\lambda = 65$). **a** time behaviour of the mean particle alignment with vorticity, $\langle |\mathbf{p} \cdot \mathbf{e}_\omega| \rangle$, **b** particle mean square rotation rate, $\langle \dot{\mathbf{p}}_i \dot{\mathbf{p}}_i \rangle / \langle \varepsilon \rangle$, as a function of particle aspect ratio, α . Labels FDNS and LES indicate a priori and a posteriori tests without particle SGS model, respectively. Labels LES+SDE and LES-ADM indicate simulations with the stochastic and the ADM-based particle SGS model, respectively. Reprinted from [22]

instances (e.g. stationary isotropic flows in the diffusive regime [82]), simplifications are possible when the physical phenomenon under investigation (e.g. near-wall clustering [93]) is characterized by timescales much longer than the correlation timescale of the velocity gradients seen: In this case, as discussed in [82], gradients can be regarded as a *fast* process, modelled as white noise (as done in [22]) and removed from the state vector. This assumption is usually made when particle orientation is modelled as a simple diffusive process or with a Fokker–Planck equation with constant diffusion coefficients (see [82] for a more detailed discussion).

5 Recent modelling advances

The previous sections provide an overview of the main modelling ideas that have been applied to LES of turbulent dispersed flows over the last two decades. The state of the art in this particular area, however, is far from being mature, and modelling advances are currently being developed. In particular, a new formalism has been recently proposed by Minier [83] to extend the LES approach to turbulent polydisperse two-phase reactive flows. The formalism extends the filtered mass density function (FMDF) approach developed by Pope and co-workers [43] for variable-density flows.

Let us consider N individual particles evolving in the flow domain, described by a state vector that includes particle position \mathbf{x}_p , particle velocity \mathbf{v}_p and fluid velocity seen \mathbf{u}_s (plus a set of suitable scalars in the case of reactive flow). The corresponding Lagrangian filtered mass density function (LFMDF) at a given time t is defined as [83]:

$$\begin{aligned} \tilde{F}_L^p(t; \mathbf{y}_p, \mathbf{V}_p, \mathbf{V}_s) &= \int \sum_{n=1}^N m_p^{(n)} G(\mathbf{y}_p - \mathbf{y}'_p) \delta(\mathbf{y}'_p - \mathbf{x}_p^{(n)}(t)) \otimes \delta(\mathbf{V}_p - \mathbf{v}_p^{(n)}(t)) \otimes \delta(\mathbf{V}_s - \mathbf{u}_s^{(n)}(t)) d\mathbf{y}' \\ &= \sum_{i=1}^N m_p^{(i)} G(\mathbf{y}_p - \mathbf{x}_p^{(i)}(t)) \otimes \delta(\mathbf{V}_p - \mathbf{v}_p^{(i)}(t)) \otimes \delta(\mathbf{V}_s - \mathbf{u}_s^{(i)}(t)) \end{aligned} \quad (31)$$

where $\tilde{\cdot}$ represents a filtered quantity (note that this notation is used here in place of subscript SGS for ease of presentation), \mathbf{y}_p , \mathbf{V}_p , and \mathbf{V}_s are the sample-space values³ corresponding to the stochastic processes \mathbf{x}_p , \mathbf{v}_p , and \mathbf{u}_s , respectively, G is the filter function, superscript (n) is the particle label, and $m_p^{(n)}$ is the mass of the n th particle. From the LFMDF, it is possible to derive the corresponding Eulerian filtered mass density function (EFMDF):

$$\tilde{F}_E^p(t, \mathbf{x}; \mathbf{V}_p, \mathbf{V}_s) \equiv \tilde{F}_L^p(t; \mathbf{y}_p = \mathbf{x}, \mathbf{V}_p, \mathbf{V}_s). \quad (32)$$

³ In stochastic modelling, a sample space is the collection of all possible outcomes of a random trial, and a stochastic variable is a function defined on a sample space.

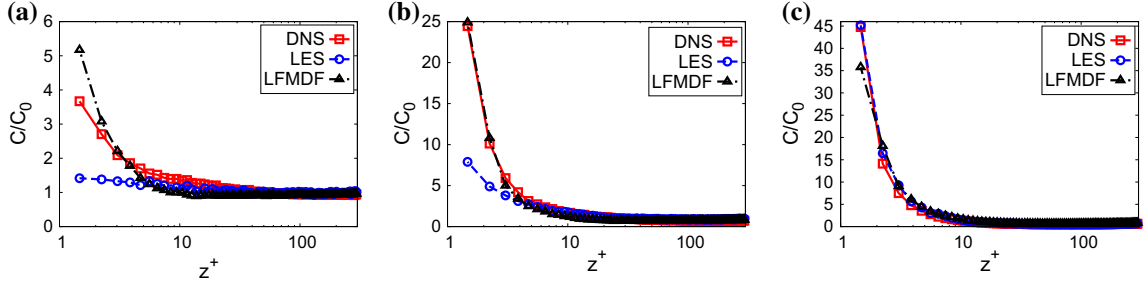


Fig. 15 Comparative assessment of the LFMDF model in particle-laden turbulent channel flow: predictions of the instantaneous particle number density at varying Stokes numbers (*triangle*) are compared with DNS results (*red square*) and with LES results with no particle SGS model (*blue circle*). **a** $St = 1$, **b** $St = 5$, **c** $St = 25$. Profiles are computed at $t^+ = 2130$ after particle injection. Reprinted from [51] with the permission of AIP Publishing (colour figure online)

Starting from the definition of \tilde{F}_L^p and \tilde{F}_E^p , it can be shown that filtered quantities can be retrieved from the EFMDF by integration over the sample-space variables. Therefore, it is important to derive the transport equations for \tilde{F}_L^p and \tilde{F}_E^p . This can be done by taking the time derivative of the fine-grained density function given by Eqs. (31) and (32). For \tilde{F}_L^p , one can derive [51,83]:

$$\frac{\partial \tilde{F}_L^p}{\partial t} = -\frac{\partial[\mathbf{V}_p \tilde{F}_L^p]}{\partial \mathbf{y}} - \frac{\partial}{\partial \mathbf{V}_p} \left[-\frac{\mathbf{V}_p - \mathbf{V}_s}{\tau_p} \tilde{F}_L^p \right] - \frac{\partial}{\partial \mathbf{V}_s} \left[\langle \tilde{\mathbf{A}}_{u_s} | \mathbf{y}_p, \mathbf{V}_p, \mathbf{u}_s \rangle \tilde{F}_L^p \right] \quad (33)$$

where $\tilde{\mathbf{A}}_{u_s} | \mathbf{y}_p$ represents the rate of change of the fluid velocity seen that needs to be modelled. The EFMDF \tilde{F}_E^p follows by definition the same transport equation as that of the LFMDF. An important point here is that \tilde{F}_E^p can be regarded as a true probabilistic density (see [82,83,85] for a detailed discussion). As such, it can, for instance, be modelled as a Fokker–Planck equation where Eq. (33) is closed as follows:

$$\begin{aligned} -\frac{\partial}{\partial \mathbf{V}_s} \left[\langle \tilde{\mathbf{A}}_{u_s} | \mathbf{y}_p, \mathbf{V}_p, \mathbf{v}_p \rangle \tilde{F}_L^p \right] &\approx -\frac{\partial}{\partial V_{s,i}} \left\{ \left[-\frac{1}{\rho} \frac{\partial \tilde{p}}{\partial x_i} + \nu \Delta \tilde{u}_i + (\tilde{v}_{p,j} - \tilde{u}_j) \frac{\partial \tilde{u}_i}{\partial x_j} - \frac{V_{s,i} - \tilde{u}_i}{(T_{L,SGS}^{\textcircled{p}})_i} \right] \tilde{F}_L^p \right\} \\ &+ \frac{1}{2} \frac{\partial^2}{\partial V_{s,i}^2} \left\{ \tilde{\epsilon} \left[C_0 b_i \frac{\tilde{k}}{\tilde{k}} + \frac{2}{3} \left(b_i \frac{\tilde{k}}{\tilde{k}} - 1 \right) \right] \tilde{F}_L^p \right\} \end{aligned} \quad (34)$$

where:

$$(T_{L,SGS}^{\textcircled{p}})_1 = \frac{T_{L,SGS}}{\sqrt{1 + \beta^2 \frac{|\tilde{\mathbf{u}}_r|^2}{2\tilde{k}/3}}}, \quad (T_{L,SGS}^{\textcircled{p}})_2 = (T_{L,SGS}^{\textcircled{p}})_3 = \frac{T_{L,SGS}}{\sqrt{1 + 4\beta^2 \frac{|\tilde{\mathbf{u}}_r|^2}{2\tilde{k}/3}}} \quad (35)$$

are the particle timescales in the longitudinal direction ($i = 1$) and in the transversal directions ($i = 2$ and $i = 3$, respectively): These timescales depend on the SGS kinetic energy \tilde{k} and on the filtered relative velocity $\tilde{\mathbf{u}}_r = \tilde{\mathbf{v}}_p - \tilde{\mathbf{u}}_s$. In addition, $\beta = T_{L,SGS}/T_{E,SGS} = T_L/T_E$ [133], and:

$$\tilde{\epsilon} = (C_S \Delta)^2 \mathcal{S}, \quad \tilde{k} = C_\epsilon (\Delta \tilde{\epsilon})^{2/3}, \quad T_{L,SGS} = \frac{\tilde{k}}{\tilde{\epsilon}} \left(\frac{1}{2} + \frac{3}{4} C_0 \right)^{-1} \quad (36)$$

where $\tilde{\epsilon}$ is the SGS dissipation rate and Δ is the filter width. The auxiliary subgrid turbulent kinetic energy is defined as follows:

$$\hat{k} = \frac{3}{2} \frac{\sum_{i=1}^3 b_i \left[\widetilde{u_{s,i}^2} - u_{s,i} \widetilde{u_{s,i}} \right]}{\sum_{i=1}^3 b_i}, \quad (37)$$

with $b_i = T_{L,SGS}/(T_{L,SGS}^{\textcircled{p}})_i$. The LFMDF transport equation is of the Fokker–Planck kind and provides all the statistical information of the state vector. However, the most convenient way to solve this equation is by a Lagrangian Monte Carlo method, since the LFMDF equation is equivalent to a system of stochastic differential

equations (SDEs) in a weak sense. This approach applies naturally to the dispersed phase since its original equations are Lagrangian. The system of SDEs corresponding to Eq. (34) reads:

$$dx_{p,i} = v_{p,i} dt, \quad (38)$$

$$dv_{p,i} = \frac{u_{s,i} - v_{p,i}}{\tau_p} dt, \quad (39)$$

$$du_{s,i} = -\frac{1}{\rho_f} \frac{\partial \tilde{p}}{\partial x_i} dt + v_f \Delta \tilde{u}_i + (\tilde{v}_{p,j} - \tilde{u}_j) \frac{\partial \tilde{u}_i}{\partial x_j} dt - \frac{u_{s,i} - \tilde{u}_i}{(T_{L,SGS})_i} dt + B_{s,ij} dW_j \quad (40)$$

where the term dW_i denotes a Wiener process, while $B_{s,ij} = \sqrt{C_i^* \tilde{\epsilon}} \delta_{ij}$ is the diffusion matrix (diagonal but not isotropic). For a more detailed description of the formalism, the reader is referred to [83, 85] and references therein. Figures 15, 16, and 17 show the predictions of the LFMDf approach in terms of concentration and near-wall segregation of inertial particles in turbulent channel flow (at $Re_\tau = 300$ based on the half channel height) [51]. A posteriori assessment made against DNS and LES without particle SGS model shows improved predictions of particle statistics, especially at intermediate Stokes numbers as demonstrated in Fig. 15 for particle number density and in Fig. 16 for particle velocity fluctuations. Regarding this last figure, note that an overshoot of all root mean square (rms) components is obtained in the case of LES without SGS model. This may be surprising, since LES is expected to give a filtered field, i.e. a field from which part of the fluctuations (mainly the highest frequency ones) has been removed by filtering. As discussed also in [72], however, this behaviour is due to the subgrid modelling error in the LES equations for the fluid phase, which leads to an overshoot of the rms of the fluid velocity components (not shown) when very coarse grids are used, as done in [51] where the LES grid is 8 times coarser than the DNS one in each spatial direction. The observed overshoot is a rather well-known behaviour of coarse LES, especially for the RMS of the streamwise component [72]. The LFMDf formalism provides a rigorous and physically sound approach to the large-eddy simulation of turbulent dispersed flows. However, it is a purely statistical approach that does not aim at recovering much as far as filtering of turbulent coherent structures is concerned. This is shown in Fig. 17, where the Voronoï diagrams of near-wall particle clusters are shown [51]. The PDFs shown in Fig. 17a clearly depart from the Poisson distribution [87], with higher probability of finding depleted regions (large Voronoï areas) and concentrated regions (small Voronoï areas), a typical signature of preferential concentration. The LFMDf model has little

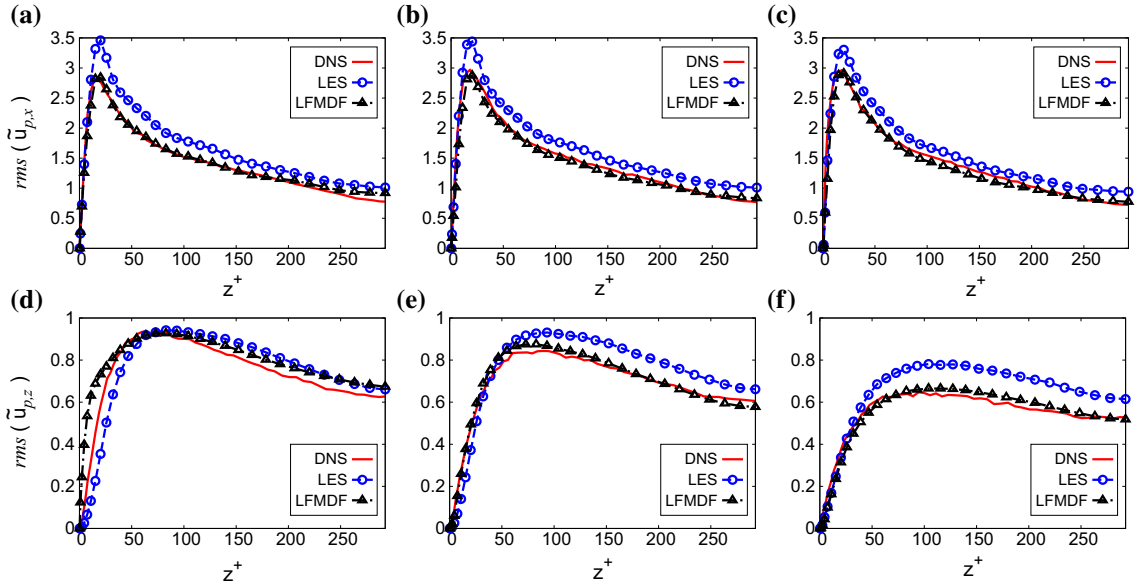


Fig. 16 Comparative assessment of the LFMDf model in particle-laden turbulent channel flow: predictions of the particle velocity rms at varying Stokes number (*black triangle*) are compared with DNS results (*red dash line*) and with LES results with no particle SGS model (*blue circle*). **a, d** $St = 1$, **b, e** $St = 5$, **c-f** $St = 25$, **a-c** streamwise component, **d-f** wall-normal component. Statistics are obtained averaging over a time window $\Delta t^+ = 1800$. Reprinted from [51] with the permission of AIP Publishing (colour figure online)

effect on the prediction of concentrated regions, and the first cross-over point, \mathcal{V}_c , representing the threshold value below which Voronoi areas are considered to belong to a cluster, occurs at slightly larger values than in DNS (see inset and Fig. 17b). Figure 17c, d provides a visualization of particle clusters (in dark grey) and particle voids (in light grey) identified using the threshold values, \mathcal{V}_c and \mathcal{V}_v , respectively, indicated in Fig. 17b. Compared to DNS, shown in Panel (c), clusters and voids in LES correspond to broader particle streaks and wider inter-cluster spacing, as shown in Panel (d).

In terms of future perspectives, there is room for improving further the quality and predictive capabilities of the approach. A first step would be the development of a dynamic procedure to determine at each time step the optimal values of the model coefficients, C_0 , appearing in Eq. (34) and C_ϵ appearing in Eq. (36), possibly as functions of the particle Stokes number. Another improvement could be represented by the implementation of higher-order closures in the Langevin equation for the fluid velocity seen by the particles. Finally, it would be very useful to implement low- Re corrections to better capture the near-wall behaviour of the statistics: This should improve the predictive capabilities of the method at relatively low particle inertia, which currently represent the weak point of the LFMDF. A different modelling approach that could be very promising is based on the use of wall functions as SGS closure for the particle phase. The idea is similar to wall-layer modelling in single-phase LES [94]: When the computational grid is so coarse that even the smallest near-wall cell contains a large number of eddies, wall-layer models treat the inner layer in a Reynolds-averaged sense (namely the layer is assumed to be governed by the Reynolds-averaged Navier–Stokes equations, rather than the filtered Navier–Stokes equations solved in LES in the outer layer), and statistical arguments can be used to represent only the average effect of near-wall turbulent structures [94]. Because of this philosophy, wall-layer models usually perform better at high Reynolds numbers, when the grid gets necessarily coarser than what DNS would require, and LES becomes the natural alternative. To the best of this author’s knowledge, no wall-layer model has been yet developed and coupled to LES to simulate particle-laden turbulent flows. In the recent study of Dupuy et al. [28], however, a candidate model has been tested (but not yet in combination with DNS) to compute the deposition of non-Brownian particles in turbulent open channel flow. The model is based on the formulation proposed by Fan and Ahmadi [29] to estimate the deposition rate of spherical particles from turbulent air streams in vertical ducts. Such formulation takes into account the existence of near-wall coherent structures (in particular quasi-streamwise vortices, sweeps, and ejections) by assuming that sweeps may be approximated by a steady plane viscous stagnation point flow in which the flow pattern is perfectly periodic in the spanwise direction and invariant in the streamwise direction [29]. The steady flow condition is justified by the time persistence of the quasi-streamwise vortices compared with their characteristic turn-around time. In addition, because sweeps and ejections are mainly responsible for particle motion to and away from the wall, only the flow pattern in the cross-flow plane is modelled. In spite of its simplicity, the model predictions in terms of deposition velocity (the only observable investigated by the authors) at varying particle-to-liquid density ratio, particle diameter, friction velocity and wall roughness for the specific case of hydrosol particles are in good agreement with the experimental results [28]. Other models that could be employed as wall-layer functions could be the stochastic models of Guingo and Minier [50] and Jin et al. [57], developed specifically to predict particle transport and deposition in turbulent boundary layers. Both are one-dimensional boundary-layer models of the fluid velocity seen that explicitly mimic particle interaction with the near-wall sweep/ejection events. In the stochastic quadrant model of Jin et al. [57], in particular, these events are captured using the quadrant analysis of Willmarth and Lu [136]. In [50], a Markovian process is used to include the same geometrical features in a statistical Lagrangian description and compute particle deposition rate in turbulent flows. In particular, a one-dimensional boundary-layer model of the velocity of the flow seen by a particle is developed to simulate explicitly particle interaction with the near-wall sweep/ejection events, which are rendered as a Markovian jump process $S(t)$ attached to each Lagrangian particle: $S(t)$ can take three possible values representing particle entrainment in a sweep or particle entrainment in an ejection or particle motion in the absence of either event. Depending on the event that carries the particle, the fluid velocity seen enters the stochastic model as either deterministic or random. Interestingly, the model is able to capture the existence of two different deposition regimes (named free-flight regime and diffusional regime), whose relative importance depends on particle inertia [50].

6 Final remarks and future perspectives

The models presented in this review cover the entire spectrum of approaches to model subgrid particle dispersion in turbulent flow. Perhaps the only general conclusion that can be safely drawn surveying the performance

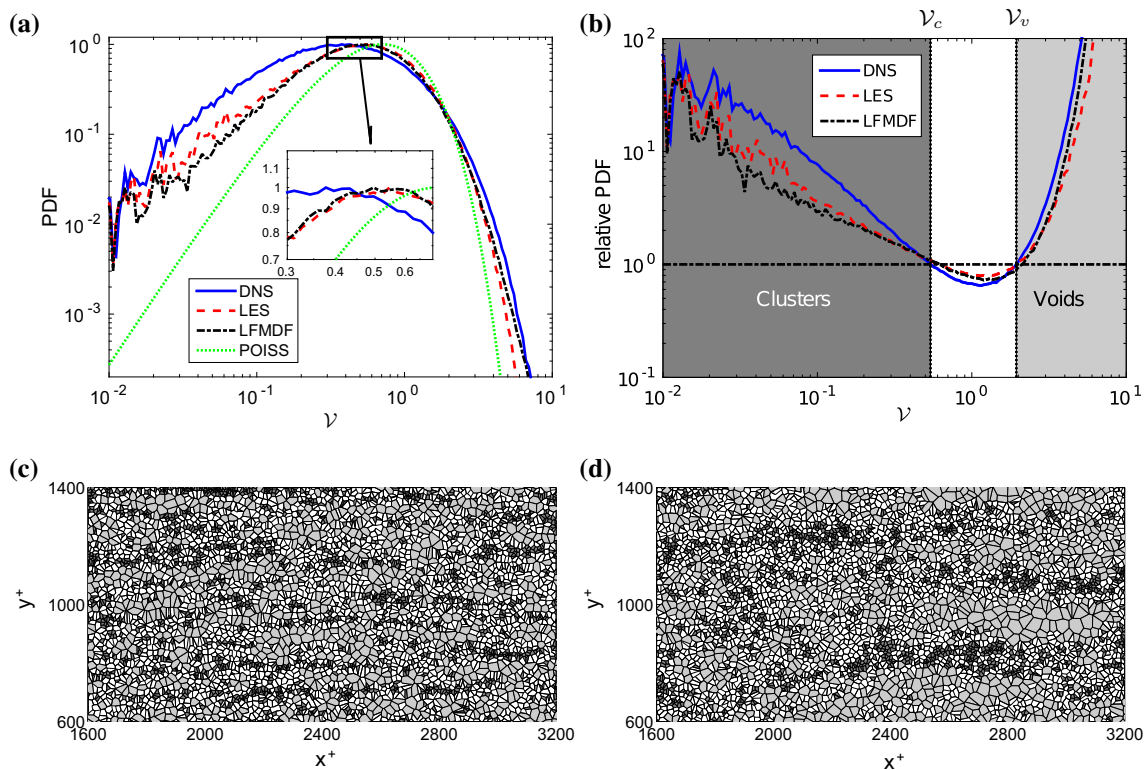


Fig. 17 PDF of normalized Voronoi areas ($\mathcal{V} = A/\bar{A}$) for $St = 5$ particles on a wall-parallel fluid slab located at distance $1 \leq z^+ \leq 5$ from the wall **(a)** and relative PDF **(b)**. LFMDF results (*dash dot dash line*) are compared with DNS results (*blue line*) and with LES results with no particle SGS model (*red dash line*). **c, d** Show the Voronoi tessellation of particle instantaneous distribution at steady state for particle concentration in DNS and in LES with LFMDF as particle SGS model, respectively. Particle clusters are in *dark grey*, and voids are in *light grey*. Reprinted from [51] with the permission of AIP Publishing (colour figure online)

of the different models is that no universal model (perhaps not even a *good-enough* model) is yet available. Whatever the choice, a necessary condition for a model is to correctly account for the physics of the problem considered, e.g. ensure the reconstruction of the SGS kinetic energy and the SGS characteristic timescale for stochastic diffusive processes, use available information on the two-point fluid velocity correlations for empirical eigenfunctions (extracted by POD [4, 130]), satisfy the incompressibility constraint and the shape of the energy spectrum at large wavenumbers in KS, ensure the conformity of the fractal dimension of velocity components with experimental data in FI. Being just the necessary condition, however, it is not always sufficient by definition.

In the context of dilute turbulent dispersed flows, the main objectives of a particle SGS model are to capture as correctly as possible particle kinetic properties but also preferential concentration phenomena determined by the small-scale interaction between inertial parcels and turbulent structures. In Lagrangian stochastic models, these objectives are achieved by modelling the unresolved part of the fluid velocity seen by the particles along their trajectory (some models consider the “whole” velocity [12], some others only the fluctuating or unresolved part [32, 81, 100]). As written by Minier [83], however, almost all available models for LES have been derived extending directly those already available for Reynolds-averaged approaches. This has led to a plethora of different formulations, each based on different assumptions (e.g local equilibrium of the SGS fluid velocity seen [81], nonzero dissipation rate of the SGS kinetic energy and negligible SGS crossing trajectory effects [32]) and different forms of the Langevin equation (namely different expressions for the drift term [12] and for the diffusion coefficient [83]). In addition, all particle SGS models provide results that depend strongly on the particle Stokes number and/or on the choice of the model timescale. This indicates that a sound theoretical framework to develop Lagrangian stochastic models for LES of turbulent dispersed flows is needed, and, only recently, efforts in this direction have been taken [82, 83]. For instance, there is still uncertainty regarding the modalities by which stochastic models should deal with the non-Gaussianity of the particle Lagrangian

velocity increments, which in turn leads to heavy-tailed probability density functions for particle acceleration [14]. Langevin-type equations cannot reproduce such features, and models must account for nonlinear drift and diffusion terms. Other open issues concern the most adequate parameterization of the SGS relaxation time in the near-wall region of wall-bounded flows and, for the sake of predicting preferential concentration-related phenomena, proper account of particle inertia (e.g. crossing trajectory) effects on the SGS time scales adopted in the model: Currently, these effects are taken into account only in few models (e.g. [31, 100]).

Structural models (fractal interpolation in particular) have been less explored compared to stochastic models. However, they have the obvious advantage of accounting for spatial correlations of the SGS fluid velocity components, which are crucial for phenomena such as pair dispersion, preferential concentration, collision, break-up, coalescence and agglomeration [105]. Future research efforts should be aimed at providing a sound assessment of the performance of structural models, particularly in high Reynolds number flows and at higher volume concentrations of the dispersed phase.

Finally, it should be noted that no systematic quantification of the computational cost of the particle SGS model compared to no-model LES and to DNS has been performed. Clearly, the model must be (significantly) less expensive than the full DNS and require limited computational overhead to become appealing (e.g. for implementation in general-purpose CFD codes). A first quantification of the numerical effort has been provided recently by Breuer and Hoppe [17], who tested an extended version of the Langevin model proposed by Pozorski and Apte [100] for bubble-laden and particle-laden channel flow. The average computational time due to the application of the model was found to increase by 15%, the increase being of about 8% when a simplified form of the diffusion matrix is used and terms preventing spurious drifts are neglected without strongly affecting the average properties of the dispersed phase. The idea behind using particle SGS models as wall-layer functions is also motivated by reasons of computational costs of the simulation. These models should extract the most relevant and most appropriate information about near-wall structures to ensure accurate prediction of macroscopic quantities such as deposition and re-entrainment rates, and should then be able to incorporate such information in a computationally efficient way.

Acknowledgements The author is very grateful to Jean-Pierre Minier and Jacek Pozorski for the useful discussions and to the reviewers for their comments and suggestions, which have significantly improved the quality of the paper.

References

1. Adams, N.A., Hickel, S., Franz, S.: Implicit subgrid-scale modeling by adaptive deconvolution. *J. Comput. Phys.* **200**, 412–431 (2004)
2. Adams, N.A.: A stochastic extension of the approximate deconvolution model. *Phys. Fluids* **23**, 055103 (2011)
3. Aguirre, C., Guo, Y., Ayrault, M.: Coupling of a subgrid Lagrangian stochastic model with large-eddy simulation. *C. R. Mech.* **332**, 627–632 (2004)
4. Allery, C., Béghein, C., Waławczyk, M., Pozorski, J.: Application of POD-based dynamical systems to dispersion and deposition of particles in turbulent channel flow. *Int. J. Multiphase Flow* **58**, 97–113 (2014)
5. Amiri, A.E., Hannani, S.K., Mashayek, F.: Large-eddy simulation of particle-laden turbulent flow with heat transfer. *Numer. Heat Trans.* **50**, 285–313 (2006)
6. Apte, S.V., Mahesh, K., Moin, P., Oefelein, J.C.: Large-eddy simulation of swirling particle-laden flows in a coaxial-jet combustor. *Int. J. Multiphase Flow* **29**, 1311–1331 (2003)
7. Apte, S.V., Gorkhovski, M., Moin, P.: LES of atomising spray with stochastic modelling of secondary breakup. *Int. J. Multiphase Flow* **29**, 1503–1522 (2003)
8. Armenio, V., Piomelli, U., Fiorotto, V.: Effect of the subgrid scales on particle motion. *Phys. Fluids* **11**, 3030 (1999)
9. Balachandar, S., Eaton, J.K.: Turbulent dispersed multiphase flows. *Ann. Rev. Fluid Mech.* **42**, 11–33 (2010)
10. Balachandar, S.: A scaling analysis for point-particle approaches to turbulent multiphase flows. *Int. J. Multiphase Flow* **35**, 801–810 (2009)
11. Bassenne, M., Urzay, J., Moin, P.: Extraction of coherent clusters in particle-laden turbulent flows using wavelet filters, pp. 107–121. *Annual Research Briefs, Center for Turbulence Research, Stanford University* (2016)
12. Berrouk, A., Laurence, D., Riley, J., Stock, D.: Stochastic modelling of inertial particle dispersion by subgrid motion for LES of high Reynolds number pipe flow. *J. Turbul.* **8**, 1–20 (2007)
13. Bianco, F., Chibbaro, S., Marchioli, C., Salvetti, M.V., Soldati, A.: Intrinsic filtering errors of Lagrangian particle tracking in LES flow fields. *Phys. Fluids* **24**, 045103 (2012)
14. Bini, M., Jones, W.P.: Particle acceleration in turbulent flows: A class of nonlinear stochastic models for intermittency. *Phys. Fluids* **19**, 035104 (2007)
15. Bini, M., Jones, W.P.: Large-eddy simulation of particle-laden turbulent flows. *J. Fluid Mech.* **614**, 207–252 (2008)
16. Boivin, M., Simonin, O., Squires, K.D.: On the prediction of gas-solid flows with two-way coupling using large eddy simulation. *Phys. Fluids* **12**, 2080–2090 (2000)
17. Breuer, M., Hoppe, F.: Influence of a cost-efficient Langevin sub-grid scale model on the dispersed phase of large-eddy simulations of turbulent bubble-laden and particle-laden flows. *Int. J. Multiphase Flow* **89**, 23–44 (2017)

18. Calzavarini, E., Donini, A., Lavezzo, V., Marchioli, C., Pitton, E., Soldati, A., Toschi, F.: On the error estimate in sub-grid models for particles in turbulent flows. In: Kuerten, J.G.M., Geurts, B., Armenio, V., Frohlich, J. (eds.) *Direct and Large-Eddy Simulation VIII*. ERCOFTAC Series, vol. 15, pp. 171–176. Springer, Dordrecht (2011)
19. Caporaloni, M., Tampieri, F., Trombetti, F., Vittori, O.: Transfer of particles in non-isotropic air turbulence. *J. Atmos. Sci.* **32**, 565–568 (1975)
20. Casciola, C.M., Gualtieri, P., Picano, F., Sardina, G., Troiani, G.: Dynamics of inertial particles in free jets. *Phys. Scr.* **T142**, 014001 (2010)
21. Cernick, M.J., Tullis, S.W., Lightstone, M.F.: Particle subgrid scale modelling in large-eddy simulations of particle-laden turbulence. *J. Turbul.* **16**, 101–135 (2015)
22. Chen, J., Jin, G., Zhang, J.: Large eddy simulation of orientation and rotation of ellipsoidal particles in isotropic turbulent flows. *J. Turbul.* **17**, 308–326 (2016)
23. Chibbaro, S., Marchioli, C., Salvetti, M.V., Soldati, A.: Particle tracking in LES flow fields: conditional Lagrangian statistics of filtering error. *J. Turbul.* **15**, 22–33 (2014)
24. Chibbaro, S., Minier, J.-P.: A note on the consistency of hybrid Eulerian/Lagrangian approach to multiphase flows. *Int. J. Multiphase Flow* **37**, 293–297 (2011)
25. Csanady, G.: Turbulent diffusion of heavy particles in the atmosphere. *J. Atmos. Sci.* **20**, 201–208 (1963)
26. Derksen, J.J., van den Akker, H.E.A., Sundaresan, S.: Two-way coupled large-eddy simulations of the gas-solid flow in cyclone separators. *AIChE J.* **54**, 872–885 (2008)
27. Dritselis, C.D., Vlachos, N.S.: Large eddy simulation of gas-particle turbulent channel flow with momentum exchange between the phases. *Int. J. Multiphase Flow* **37**, 706–721 (2011)
28. Dupuy, M., Xayasenh, A., Duval, H., Waz, E.: Analysis of non-Brownian particle deposition from turbulent liquid-flow. *AIChE J.* **62**, 891–904 (2016)
29. Fan, F.-G., Ahmadi, G.: A sublayer model for turbulent deposition of particles in vertical ducts with smooth and rough surfaces. *J. Aerosol Sci.* **24**, 45–64 (1993)
30. Fede, P., Simonin, O., Villedieu, P.: Monte-Carlo simulation of colliding particles or coalescing droplets transported by a turbulent flow in the framework of a joint fluid-particle pdf approach. *Int. J. Multiphase Flow* **74**, 165–183 (2015)
31. Fede, P., Simonin, O.: Numerical study of the subgrid fluid turbulence effects on the statistics of heavy colliding particles. *Phys. Fluids* **18**, 045103 (2006)
32. Fede, P., Simonin, O., Villedieu, P., Squires, K.D.: Stochastic modelling of the turbulent subgrid fluid velocity along inertial particle trajectories. In: *Proceedings of Summer Program, Center for Turbulence Research, Stanford University*, pp. 22–33 (2006)
33. Fessler, J.R., Kulick, J.D., Eaton, J.K.: Preferential concentration of heavy-particles in a turbulent channel flow. *Phys. Fluids* **6**, 3742–3749 (1994)
34. Flohr, P., Vassilicos, J.C.: A scalar subgrid model with flow structure for large-eddy simulations of scalar variances. *J. Fluid Mech.* **407**, 315–349 (2000)
35. Fox, R.O.: Large-eddy-simulation tools for multiphase flows. *Ann. Rev. Fluid Mech.* **44**, 47–76 (2012)
36. Fukagata, K., Zahrai, S., Bark, F.: Dynamics of Brownian particles in a turbulent channel flow. *Heat Mass Transf.* **40**, 715–726 (2004)
37. Fung, J.C.H., Hunt, J.C.R., Malik, N.A., Perkins, R.J.: Kinematic simulation of homogeneous turbulence by unsteady random Fourier modes. *J. Fluid Mech.* **236**, 281–318 (1992)
38. Gagnol, R.: The Faxén formulae for a rigid sphere in an unsteady non-uniform Stokes flow. *J. Méch. Théor. Appl.* **1**, 143–160 (1983)
39. Geurts, B.J., Kuerten, J.G.M.: Ideal stochastic forcing for the motion of particles in large-eddy simulation extracted from direct numerical simulation of turbulent channel flow. *Phys. Fluids* **24**, 081702 (2012)
40. Germano, M.: Turbulence: the filtering approach. *J. Fluid Mech.* **238**, 325–336 (1992)
41. Germano, M.: Differential filters for the large-eddy numerical simulation of turbulent flows. *Phys. Fluids* **29**, 1755–1757 (1986)
42. Germano, M.: Differential filters of elliptic type. *Phys. Fluids* **29**, 1757–1758 (1986)
43. Gicquel, L.Y.M., Givi, P., Jaber, F.A., Pope, S.B.: Velocity filtered density function for large eddy simulation of turbulent flows. *Phys. Fluids* **14**, 1196–1213 (2002)
44. Gobert, C., Manhart, M.: Subgrid modelling for particle-LES by spectrally optimised interpolation (SOI). *J. Comput. Phys.* **230**, 7796–7820 (2011)
45. Gobert, C., Manhart, M.: A-priori and a-posteriori analysis of models for large-eddy simulation of particle-laden flow. *Phys. Fluid Dyn.* **1004**, 1–18 (2011)
46. Gobert, C.: Analytical assessment of models for large eddy simulation of particle laden flow. *J. Turbul.* **11**, 1–24 (2010)
47. Gualtieri, P., Casciola, C.M., Benzi, R., Piva, R.: Preservation of statistical properties in large-eddy simulation of shear turbulence. *J. Fluid Mech.* **592**, 471–494 (2007)
48. Gualtieri, P., Picano, F., Sardina, G., Casciola, C.M.: Statistics of particle pair relative velocity in the homogeneous shear flow. *Phys. D* **241**, 245–250 (2012)
49. Guha, A.: Transport and deposition of particles in turbulent and laminar flow. *Ann. Rev. Fluid Mech.* **40**, 311–341 (2008)
50. Guingo, M., Minier, J.-P.: A stochastic model of coherent structures for particle deposition in turbulent flows. *Phys. Fluids* **20**, 053303 (2008)
51. Innocenti, A., Marchioli, C., Chibbaro, S.: Lagrangian filtered density function for LES-based stochastic modelling of turbulent dispersed flows. *Phys. Fluids* **27**, 053305 (2016)
52. Jeffery, G.B.: The motion of ellipsoidal particles immersed in a viscous flow. *Proc. R. Soc. A* **102**, 161–179 (1922)
53. Jin, G., He, G.-W., Wang, L.-P.: Large-eddy simulation of turbulent collision of heavy particles in isotropic turbulence. *Phys. Fluids* **22**, 055106 (2010)
54. Jin, G., He, G.-W., Wang, L.-P., Zhang, J.: Subgrid scale fluid velocity timescales seen by inertial particles in large-eddy simulation of particle-laden turbulence. *Int. J. Multiphase Flow* **36**, 432–437 (2010)

55. Jin, G., He, G.-W.: A nonlinear model for the subgrid timescale experienced by heavy particles in large-eddy simulation of isotropic turbulence with a stochastic differential equation. *New J. Phys.* **15**, 035011 (2010)
56. Jin, G., Zhang, J., He, G.-W., Wang, L.-P.: Assessment of large-eddy simulation in capturing preferential concentration of heavy particles in isotropic turbulent flows. *Phys. Scr.* **T142**, 014061 (2010)
57. Jin, C., Potts, I., Reeks, M.W.: A simple stochastic quadrant model for the transport and deposition of particles in turbulent boundary layers. *Phys. Fluids* **27**, 053305 (2015)
58. Kenjeres, S.: On recent progress in modelling and simulations of multi-scale transfer of mass, momentum and particles in bio-medical applications. *Flow Turbul. Combust.* **96**, 837–860 (2016)
59. Khan, M.A.I., Luo, X.Y., Nicolleau, F.C.G.A., Tucker, P.G., Lo Iacono, G.: Effects of LES sub-grid flow structure on particle deposition in a plane channel with a ribbed wall. *Int. J. Numer. Methods. Biomed. Eng.* **26**, 999–1015 (2010)
60. Knorps, M., Pozorski, J.: An inhomogeneous stochastic subgrid model for particle dispersion in Large-Eddy Simulation. In: *Direct and Large-Eddy Simulation IX* (Eds.: Fröhlich J. et al.), pp. 671–678 (2015)
61. Kuerten, J.G.M.: Point-particle DNS and LES of particle-laden turbulent flow—a state-of-the-art review. *Flow Turbul. Combust.* **97**, 689–713 (2016)
62. Kuerten, J.G.M.: Subgrid modeling in particle-laden channel flow. *Phys. Fluids* **18**, 025108 (2006)
63. Kuerten, J.G.M., Vreman, A.W.: Can turbophoresis be predicted by large-eddy simulation? *Phys. Fluids* **17**, 011701 (2005)
64. Lazaro, B.J., Lasheras, J.C.: Particle dispersion in the developing free shear layer. Part 1. Unforced flow. *J. Fluid Mech.* **235**, 135–178 (1992)
65. Lazaro, B.J., Lasheras, J.C.: Particle dispersion in the developing free shear layer. Part 2. Forced flow. *J. Fluid Mech.* **235**, 179–221 (1992)
66. Lessani, B., Nakhaei, M.H.: Large-eddy simulation of particle-laden turbulent flow with heat transfer. *Int. J. Heat Mass Transf.* **67**, 974–983 (2003)
67. Le Ribault, C., Simoons, S., Vinkovic, I.: Hybrid large eddy simulation/Lagarangian stochastic model for turbulent passive and reactive scalar dispersion in a plane jet. *Chem. Eng. Commun.* **199**, 435–460 (2012)
68. Lu, H., Rutland, C.J.: Structural subgrid-scale modeling for large-eddy simulation: a review. *Acta Mech. Sin.* **32**, 567–578 (2016)
69. Mallouppas, G., van Wachem, B.: Large eddy simulations of turbulent particle-laden channel flow. *Int. J. Multiphase Flow* **54**, 65–75 (2013)
70. Marchioli, C., Armenio, V., Salvetti, M.V., Soldati, A.: Mechanisms for deposition and resuspension of heavy particles in turbulent flow over wavy interfaces. *Phys. Fluids* **18**, 025102 (2006)
71. Marchioli, C., Picciotto, M., Soldati, A.: Particle dispersion and wall-dependent fluid scales in turbulent bounded flow: implications for local equilibrium models. *J. Turbul.* **7**, 1–12 (2006)
72. Marchioli, C., Salvetti, M.V., Soldati, A.: Appraisal of energy recovering sub-grid scale models for large-eddy simulation of turbulent dispersed flows. *Acta Mech.* **201**, 277–296 (2008)
73. Marchioli, C., Salvetti, M.V., Soldati, A.: Some issues concerning large-eddy simulation of inertial particle dispersion in turbulent bounded flows. *Phys. Fluids* **20**, 040603 (2008)
74. Marchioli, C., Soldati, A.: Mechanisms for particle transfer and segregation in turbulent boundary layer. *J. Fluid Mech.* **468**, 283–315 (2002)
75. Marchioli, C., Soldati, A.: Rotation statistics of fibers in wall shear turbulence. *Acta Mech.* **224**, 2311–2329 (2013)
76. Marchioli, C., Soldati, A., Kuerten, J.G.M., Arcen, B., Taniere, A., Goldensohn, G., Squires, K.D., Cargnelutti, M.F., Portela, L.M.: Statistics of particle dispersion in direct numerical simulations of wall-bounded turbulence: results of an international collaborative benchmark test. *Int. J. Multiphase Flow* **34**, 879–893 (2008)
77. Marchioli, C., Soldati, A., Salvetti, M.V., Kuerten, J.G.M., Konan, A., Fede, P., Simonin, O., Squires, K.D., Gobert, C., Manhart, M., Jaszczur, M., Portela, L.M.: Benchmark test on particle-laden channel flow with point-particle LES. In: *Kuerten, J.G.M., Geurts, B., Armenio, V., Fröhlich, J. (eds.) Direct and Large-Eddy Simulation VIII. ERCOFTAC Series*, vol. 15, pp. 177–182. Springer, Dordrecht (2011)
78. Mason, P.J.: Large-eddy simulation: a critical review of the technique. *Q. J. R. Meteorol. Soc.* **120**, 1–26 (1994)
79. Maxey, M., Riley, J.: Equation of motion for a small rigid sphere in a nonuniform flow. *Phys. Fluids* **26**, 883–889 (1983)
80. Meneveau, C., Katz, J.: Scale-invariance and turbulence models for large-eddy simulation. *Ann. Rev. Fluid Mech.* **32**, 1–32 (2000)
81. Michalek, W.R., Kuerten, J.G.M., Liew, R., Zeegers, C.H., Pozorski, J., Geurts, B.J.: A hybrid deconvolution stochastic model for LES of particle-laden flow. *Phys. Fluids* **25**, 123202 (2013)
82. Minier, J.-P.: Statistical description of polydisperse turbulent two-phase flows. *Phys. Rep.* **665**, 1–122 (2016)
83. Minier, J.-P.: On Lagrangian stochastic methods for turbulent polydispersed two-phase reactive flows. *Prog. Energy Combust. Sci.* **50**, 1–62 (2015)
84. Minier, J.-P., Profeta, C.: Kinetic and dynamic probability-density-function descriptions of turbulent dispersed two-phase flows. *Phys. Rev. E* **92**, 053020 (2015)
85. Minier, J.-P., Chibbaro, S., Pope, S.B.: Guidelines for the formulation of Lagrangian stochastic models for particle simulations of single-phase and dispersed two-phase turbulent flows. *Phys. Fluids* **26**, 113303 (2014)
86. Minier, J.-P., Peirano, E.: The PDF approach to turbulent polydispersed two-phase flows. *Phys. Rep.* **352**, 1–214 (2001)
87. Monchaux, R., Bourgoin, M., Cartellier, A.: Preferential concentration of heavy particles: a Voronoï analysis. *Phys. Fluids* **22**, 103304 (2010)
88. Oefelein, J.C.: Large eddy simulation of turbulent combustion processes in propulsion and power systems. *Phys. Fluids* **42**, 2–37 (2006)
89. Park, G.I., Bassenne, M., Urzay, J., Moin, P.: A simple dynamic subgrid-scale model for LES of particle-laden turbulence. *Phys. Rev. Fluids* **2**, 024302 (2017)
90. Park, G.I., Urzay, J., Bassenne, M., Moin, P.: A dynamic subgrid-scale model based on differential filters for LES of particle-laden turbulent flows, pp. 17–26. Annual Research Briefs, Center for Turbulence Research, Stanford University (2015)

91. Peirano, E., Chibbaro, S., Pozorski, J., Minier, J.-P.: Mean-field/PDF numerical approach for polydispersed turbulent two-phase flows. *Prog. Energy Combust. Sci.* **32**, 315–371 (2006)
92. Pasmazoglou, I., Kempf, A.M., Martinez, S.N.: A dynamic model for the Lagrangian stochastic dispersion coefficient. *Phys. Fluids* **25**, 125108 (2013)
93. Picciotto, M., Marchioli, C., Soldati, A.: Characterization of near-wall accumulation regions for inertial particles in turbulent boundary layers. *Phys. Fluids* **17**, 098101 (2005)
94. Piomelli, U., Balaras, E.: Wall-layer models for large-eddy simulations. *Annu. Rev. Fluid Mech.* **34**, 349–374 (2002)
95. Pitsch, H.: Large-eddy simulation of turbulent combustion. *Ann. Rev. Fluid Mech.* **38**, 453–482 (2006)
96. Pope, S.: Ten questions concerning the large-eddy simulation of turbulent flows. *New J. Phys.* **6**, 35 (2004)
97. Pope, S.: Lagrangian PDF methods for turbulent flows. *Annu. Rev. Fluid Mech.* **26**, 23–63 (1994)
98. Pozorski, J.: Models of turbulent flows and particle dynamics. In: Minier, J.P., Pozorski, J. (eds.) *Particles in Wall-Bounded Turbulent Flows: Deposition, Resuspension and Agglomeration*. CISM International Centre for Mechanical Sciences, vol. 571, pp. 97–150. Springer, Wien (2017)
99. Pozorski, J., Knorps, M., Minier, J.-P., Kuerten, J.G.M.: Anisotropic stochastic dispersion model for LES of particle-laden turbulent flows. In: *Proceedings of Engineering Turbulence Modeling and Measurements*, vol. 9, Thessaloniki, Greece, 6–8 June (2012)
100. Pozorski, J., Apte, S.V.: Filtered particle tracking in isotropic turbulence and stochastic modeling of subgrid-scale dispersion. *Int. J. Multiphase Flow* **35**, 118–128 (2009)
101. Pozorski, J., Waclawczyk, T., Luniewski, M.: LES of turbulent channel flow and heavy particle dispersion. *J. Theor. Appl. Mech.* **45**, 643–657 (2007)
102. Pozorski, J., Luniewski, M.: Analysis of SGS particle dispersion model in LES of channel flow. *Quality and Reliability of LES* 331–342 (2008)
103. Raman, V., Fox, R.O.: Modeling of fine-particle formation in turbulent flames. *Ann. Rev. Fluid Mech.* **48**, 159–190 (2016)
104. Rasam, A., Pouransari, Z., Vervisch, L., Johansson, A.V.: Assessment of subgrid-scale stress statistics in non-premixed turbulent wall-jet flames. *J. Turbul.* **17**, 471–490 (2016)
105. Ray, B., Collins, L.R.: Investigation of sub-Kolmogorov inertial particle pair dynamics in turbulence using novel satellite particle simulations. *J. Fluid Mech.* **720**, 192–211 (2013)
106. Ray, B., Collins, L.R.: A subgrid model for clustering of high-inertia particles in large-eddy simulations of turbulence. *J. Turbul.* **15**, 366–385 (2014)
107. Ray, B., Collins, L.R.: Preferential concentration and relative velocity statistics of inertial particles in Navier-Stokes turbulence with and without filtering. *J. Fluid Mech.* **680**, 488–510 (2011)
108. Reeks, M.W.: The transport of discrete particles in inhomogeneous turbulence. *J. Aerosol Sci.* **14**, 729–739 (1983)
109. Keshevarzi, Reza: A., Nagi Ziaei, A., Homayoun, E., Shirvani, A.: Fractal-Markovian scaling of turbulent bursting processes in open channel flows. *Chaos Solitons Fractals* **25**, 307–318 (2005)
110. Rosa, B., Pozorski, J.: Analysis of subfilter effects on inertial particles in forced isotropic turbulence. In: *Proceedings 9th International Conference on Multiphase Flows*, pp. 1–5. Firenze, Italy (2016)
111. Sabel'nikov, V., Chtab-Desportes, A., Gorkhovski, M.: New sub-grid stochastic acceleration model in LES of high-Reynolds-number flows. *Eur. Phys. J. B* **80**, 177–187 (2011)
112. Salazar, J.P.L.C., de Jong, J., Cao, L., Woodward, S.H., Meng, H., Collins, L.R.: Experimental and numerical investigation of inertial particle clustering in isotropic turbulence. *J. Fluid Mech.* **600**, 245–256 (2008)
113. Salmanzadeh, M., Rahnama, M., Ahmadi, G.: Effect of sub-grid scales on large eddy simulation of particle deposition in a turbulent channel flow. *Aerosol Sci. Tech.* **44**, 796–806 (2010)
114. Scotti, A., Meneveau, C.: A fractal interpolation model for large-eddy simulation of turbulent flows. *Phys. D* **127**, 198–232 (1999)
115. Sengupta, K., Shotorban, B., Jacobs, G.B., Mashayek, F.: Spectral-based simulations of particle-laden turbulent flows. *Int. J. Multiphase Flow* **35**, 811–826 (2009)
116. Shotorban, B., Mashayek, F.: A stochastic model for particle motion in large-eddy simulation. *J. Turbul.* **7**, 1–13 (2006)
117. Shotorban, B., Mashayek, F.: Modeling subgrid-scale effects on particles by approximate deconvolution. *Phys. Fluids* **17**, 081701 (2005)
118. Shotorban, B., Zhang, K.K.Q., Mashayek, F.: Improvement of particle concentration prediction in large-eddy simulation by defiltering. *Int. J. Heat Mass Transf.* **50**, 3728–3739 (2007)
119. Smagorinsky, J.: General circulation experiments with the primitive equations. I. The basic experiment. *Mon. Weather Rev.* **48**, 41–71 (1963)
120. Soldati, A.: Particles-turbulence interactions in boundary layers. *ZAMM—J. Applied Math. Mech.* **85**, 683–699 (2005)
121. Soldati, A., Marchioli, C.: Sediment transport in steady turbulent boundary layers: potentials, limitations, and perspectives for Lagrangian tracking in DNS and LES. *Adv. Water Resour.* **48**, 18–30 (2012)
122. Soldati, A., Marchioli, C.: Physics and modelling of turbulent particle deposition and entrainment: review of a systematic study. *Int. J. Multiphase Flow* **35**, 827–839 (2009)
123. Stolz, P., Adams, N.A., Kleiser, L.: An approximate deconvolution model for large-eddy simulation with application to incompressible wall-bounded flows. *Phys. Fluids* **13**, 997–1015 (2001)
124. Subramanian, S.: Lagrangian-Eulerian methods for multiphase flows. *Prog. Energy Combust. Sci.* **39**, 215–245 (2013)
125. Urzay, J., Bassenne, M., Park, G.I., Moin, P.: Characteristic regimes of subgrid-scale coupling in LES of particle-laden turbulent flows. In: *Proceedings of Summer Program, Center for Turbulence Research, Stanford University*, pp. 3–13 (2014)
126. Vinkovic, I., Aguirre, C., Ayrault, M., Simoens, S.: Large-eddy simulation of the dispersion of solid particles in a turbulent boundary layer. *Bound. Layer Meteorol.* **121**, 283–311 (2006)
127. Vinkovic, I., Aguirre, C., Simoens, S.: Large-eddy simulation and Lagrangian stochastic modeling of passive scalar dispersion in a turbulent boundary layer. *J. Turbul.* **7**, 1–14 (2006)
128. Vinkovic, I., Doppler, D., Lelouvetel, J., Buffat, M.: Direct numerical simulation of particle interaction with ejections in turbulent channel flows. *Int. J. Multiphase Flow* **37**, 187–197 (2011)

129. Voth, G., Soldati, A.: Anisotropic particles in turbulence. *Ann. Rev. Fluid Mech.* **49**, 249–276 (2017)
130. Waclawczyk, M., Pozorski, J.: Two-point velocity statistics and the POD analysis of the near-wall region in a turbulent channel flow. *J. Theor. Appl. Mech.* **40**, 895–916 (2002)
131. Wang, Q., Squires, K.D.: Large eddy simulation of particle-laden turbulent channel flow. *Phys. Fluids* **8**, 1207–1223 (1996)
132. Wang, Q., Squires, K.D., Simonin, O.: Large eddy simulation of turbulent gas-solid flows in a vertical channel and evaluation of second-order models. *Int. J. Heat Mass Transf.* **19**, 505–511 (1998)
133. Wang, Q., Stock, D.: Dispersion of heavy particles by turbulent motion. *J. Atmos. Sci.* **50**, 1897–1913 (1993)
134. Weil, J., Sullivan, P., Moeng, C.: The use of large-eddy simulations in Lagrangian particle dispersion models. *J. Atmos. Sci.* **61**, 2877–2887 (2004)
135. Wells, M., Stock, D.: The effects of crossing trajectories on the dispersion of particles in a turbulent flow. *J. Fluid Mech.* **136**, 31–62 (1983)
136. Willmarth, W.W., Lu, S.S.: Structure of the Reynolds stress near the wall. *J. Fluid Mech.* **55**, 65–92 (1972)
137. Yang, Y., He, G.-W., Wang, L.-P.: Effects of subgrid-scale modeling on Lagrangian statistics in large-eddy simulation. *J. Turbul.* **9**, 1–24 (2008)
138. Yeh, F., Lei, U.: On the motion of small particles in a homogeneous isotropic turbulent flow. *Phys. Fluids A* **3**, 2571–2586 (1991)
139. Yeh, F., Lei, U.: On the motion of small particles in a homogeneous turbulent shear flow. *Phys. Fluids A* **3**, 2758–2776 (1991)
140. Yi, C., Li, J., Liu, Z.-H., Wang, L., Zheng, C.-G.: Subgrid-scale fluid statistics along the inertial particle trajectory in isotropic turbulence. *Chin. Phys. Lett.* **29**, 094701 (2012)
141. Yoshizawa, A.: A statistically-derived subgrid model for the large-eddy simulation of turbulence. *Phys. Fluids* **25**, 1532–1538 (1982)
142. Zaichik, L.I., Alipchenkov, V.M., Sinaiski, E.G.: *Particles in Turbulent Flows*. Wiley-VCH, Weinheim (2008)
143. Zamansky, R., Vinkovic, I., Gorokhovski, M.: Acceleration in turbulent channel flow: universalities in statistics, subgrid stochastic models and an application. *J. Fluid Mech.* **721**, 627–668 (2013)
144. Zhou, L.: Advances in studies on turbulent dispersed multiphase flows. *Chin. J. Chem. Eng.* **18**, 889–898 (2010)